Title

Future changes in extreme precipitation over the San Francisco Bay Area: Dependence on atmospheric river and extratropical cyclone events

Authors

Patricola, Christina M

Wehner, Michael F

Bercos-Hickey, Emily

et al.

Publication Date

2022-06-01

DOI

10.1016/j.wace.2022.100440

Peer reviewed

Weather and Climate Extremes 36 (2022) 100440

Contents lists available at ScienceDirect

Weather and Climate Extremes

journal homepage: www.elsevier.com/locate/wace

Future changes in extreme precipitation over the San Francisco Bay Area: Dependence on atmospheric river and extratropical cyclone events

Christina M. Patricola [a,b,*], Michael F. Wehner [c], Emily Bercos-Hickey [b], Flor Vanessa Maciel [d,b], Christine May [e], Michael Mak [e], Olivia Yip [f,e], Anna M. Roche [g], Susan Leal [h]

[a] Department of Geological and Atmospheric Sciences, Iowa State University, Ames, IA, USA
[b] Climate and Ecosystem Sciences Division, Lawrence Berkeley National Laboratory, Berkeley, CA, USA
[c] Computational Research Division, Lawrence Berkeley National Laboratory, Berkeley, CA, USA
[d] San Jose State University, Department of Meteorology and Climate Science, San Jose, CA, USA
[e] Pathways Climate Institute, San Francisco, CA, USA
[f] Department of Civil and Environmental Engineering, San Jose State University, San Jose, CA, USA
[g] San Francisco Public Utilities Commission, San Francisco, CA, USA
[h] Urban Water Works, San Francisco, CA, USA

ARTICLE INFO

Keywords:
Extreme precipitation
Climate change
Precipitation scaling
Clausius-Clapeyron
Atmospheric rivers
Extratropical cyclones

ABSTRACT

Extreme precipitation poses a major challenge for local governments, including the City and County of San Francisco, California, as flooding can damage and destroy infrastructure and property. As the climate continues to warm, reliable future precipitation projections are needed to provide the best possible information to decision makers. However, future changes in the magnitude of extreme precipitation are uncertain, as current state-of-the-art global climate models are typically run at relatively coarse horizontal resolutions that require the use of convective parameterization and have difficulty simulating observed extreme rainfall rates. Here, we performed ensembles of convection-permitting regional climate model simulations to investigate how five historically impactful extreme precipitation events over the San Francisco Bay Area could change if similar events occurred in future climates. We found that changes in storm-total precipitation depend strongly on storm type. Precipitation associated with an atmospheric river (AR) accompanied by an extratropical cyclone (ETC) is projected to increase at a rate exceeding (by up to 1.5 times) the theoretical Clausius Clapeyron scaling of 6–7% per °C warming. On the other hand, future precipitation changes are weak or negative for events characterized by an AR only, despite increases in precipitable water and integrated vapor transport that are similar to those of the co-occurring AR and ETC events. The differences in the sign of future precipitation change between AR-only events and co-occurring AR and ETC events is instead linked with changes in mid-tropospheric vertical velocity. Given that the majority of observed ARs are associated with an ETC, this research has important implications for future precipitation impacts over the Bay Area, as it indicates that storm-total precipitation associated with the most common type of storm event may increase by up to 26–37% in 2100 relative to historical.

1. Introduction

Water is both a necessary resource and a potential hazard for society. Too little water creates challenges for agricultural, residential, and municipal activities, whereas too much water can lead to property and infrastructure damage from flooding and landslides. The San Francisco Bay Area is susceptible to water as a hazard, as its proximity to the ocean makes it vulnerable to storm surge and sea-level rise, challenges currently under investigation as part of the San Francisco Sea Level Rise Action Plan (Kelley et al., 2016). An additional compounding problem is extreme precipitation, which is typically associated with multi-day atmospheric river events and extratropical cyclones, and is the focus of this study.

Atmospheric rivers (ARs) are long, narrow filaments of atmospheric water vapor transport often associated with an extratropical cyclone (e.g., Gimeno et al., 2014; Zhang et al., 2019) and are capable of producing heavy precipitation over land lasting for several days. Given the importance of ARs to precipitation over the western US (e.g., Dettinger,

* Corresponding author. Iowa State University, 3017 Agronomy Hall, 716 Farm House Ln, Ames, IA, 50011, USA.
E-mail address: cmp28@iastate.edu (C.M. Patricola).

https://doi.org/10.1016/j.wace.2022.100440
Received 19 July 2021; Received in revised form 25 February 2022; Accepted 5 April 2022
Available online 8 April 2022

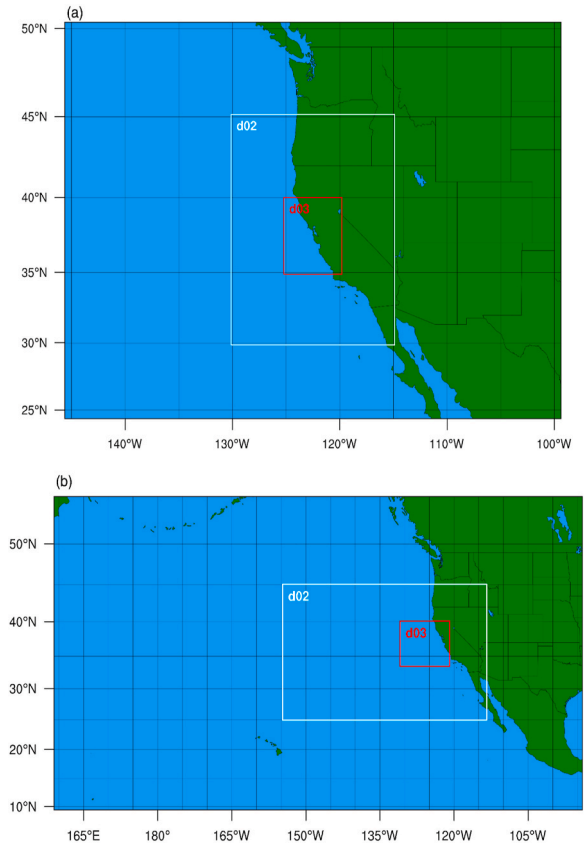

Fig. 1. The two regional climate model domain configurations that were tested for this study, namely (a) domain 1 and (b) domain 2. The regions marked d01, d02, and d03 use 27 km, 9 km, and 3 km horizontal resolution, respectively. Domain 1 was selected to perform the full set of simulations.

Table 1
List of storm events and dates with initial condition dates for the historical simulations.

Storm number	Storm type	Event dates	Simulation initial condition dates
Storm 1a	AR and ETC	Dec 2–6, 2014	Nov 28, 2014: 00z, 03z, 06z, 09z, 12z, 15z, 18z, 21z; Nov 29, 2014: 00z, 03z
Storm 1b	AR and ETC	Dec 11–12, 2014	Dec 7, 2014: 00z, 03z, 06z, 09z, 12z, 15z, 18z, 21z; Dec 8, 2014: 00z, 03z
Storm 2	AR	Jan 3–5, 1982	Dec 30, 1981: 00z, 03z, 06z, 09z, 12z, 15z, 18z, 21z; Dec 31, 1981: 00z, 03z
Storm 3	AR	Nov 4–7, 1994	Oct 31, 1994: 00z, 03z, 06z, 09z, 12z, 15z, 18z, 21z; Nov 1, 1994: 00z, 03z
Storm 4	AR and ETC	Jan 31 - Feb 8, 1998	Jan 27, 1998: 00z, 03z, 06z, 09z, 12z, 15z, 18z, 21z; Jan 28, 1998: 00z, 03z
Storm 5	AR and ETC	Dec 10–13, 1995	Dec 6, 1995: 00z, 03z, 06z, 09z, 12z, 15z, 18z, 21z; Dec 7,, 1995: 00z, 03z

2011; Lamjiri et al. 2018), there is great interest in improving their sub-seasonal to seasonal prediction and understanding how they are influenced by climate variability, such as the El Niño - Southern Oscillation (ENSO), Madden-Julian Oscillation (MJO), and quasi-biennial oscillation (QBO) (e.g., Baggett et al. 2017; Mundhenk et al. 2018; Zhou and Kim 2018; DeFlorio et al., 2019; Huang et al., 2021; Nardi et al., 2020; Patricola et al., 2020; Hagos et al., 2021). Furthermore, any

Table 2
List of physical parameterizations and model domains tested to optimize the regional model configuration. X denotes a test that was performed. Planetary boundary layer schemes include Mellor-Yamada-Janjic (MYJ) and Yonsei University (YSU). WSM6 denotes the WRF Single-Moment 6-Class Microphysics Scheme.

Parameterization test	Microphysics	Planetary boundary layer	Domain 1	Domain 2
1	Goddard	MYJ	X	
2	Goddard	YSU	X	X
3	Kessler	MYJ	X	
4	Kessler	YSU	X	X
5	Morrison	MYJ	X	
6	Morrison	YSU	X	X
7	Purdue Lin	MYJ	X	
8	Purdue Lin	YSU	X	
9	WSM6	MYJ	X	X

future changes in ARs will have important implications for precipitation. There is a consensus that western US AR frequency is expected to increase in the future, accompanied by increased precipitation (review paper by Payne et al., 2020; Dettinger, 2011; Dominguez et al., 2018; Espinoza et al., 2018; Gao et al., 2015, 2016; Gershunov et al., 2017, Gershunov et al., 2019; Hagos et al., 2016; Payne and Magnusdottir 2015; Pierce et al., 2013; Polade et al., 2017; Shields and Kiehl 2016; Swain et al., 2018; Warner et al., 2015), although the magnitude of the increase can depend on AR tracking algorithm (Shields et al., 2018). Projected increases in future extreme precipitation over western North America have been linked almost entirely to ARs (Gershunov et al., 2019), highlighting the importance of understanding these types of storms. Furthermore, using the recently developed impacts-relevant AR category scale (Ralph et al., 2019), Rhoades et al. (2020) found that future increases in the integrated vapor transport (IVT) of ARs leads to a shift in AR category from predominantly "mostly or primarily beneficial" to "mostly or primarily hazardous." However, despite the connection between ARs and extreme precipitation, a simulation of a particular AR event in the current and a warmer climate revealed that future increases in IVT did not lead to generalized increases in regional precipitation (Dominguez et al., 2018), indicating the utility of investigating both ARs and the precipitation they deliver to more fully understand future impacts.

Although future change in precipitation is a topic of global concern and has been the focus of substantial research, projections remain uncertain for several reasons. First is the possibility that extreme precipitation can change in a way that deviates from simple theory. Based solely on thermodynamic principles, a fully saturated atmosphere can hold 6–7% more moisture per ^{o}C of warming at observed near-surface air temperatures of the Earth, as established by the Clausius-Clapeyron (CC) relationship. This property of the saturation specific humidity provides a starting point to estimate extreme precipitation changes in the future. However, the change in extreme precipitation with temperature (hereon called "precipitation scaling") can deviate from the CC rate due to factors including changes in atmospheric relative humidity, storm dynamics, and cloud physics. For example, precipitation scaling that exceeds CC may be explained by positive feedbacks associated with convection, latent heat release, vertical motion, convergence, and large-scale circulation (Lenderink et al., 2017). Therefore, using CC as a "back-of-the-envelope" estimate for future changes in extreme precipitation may be insufficient to inform decisions intended to mitigate the impacts of climate change.

Several studies have investigated the scaling of precipitation with temperature, with results ranging from below to above the CC scaling rate (or "sub-CC" to "super-CC") and often depending on the temporal resolution of precipitation (e.g., Haerter et al., 2010). Global climatological mean precipitation has been found to scale below CC, increasing by about 1–3% per ^{o}C of atmospheric warming due to energy budget

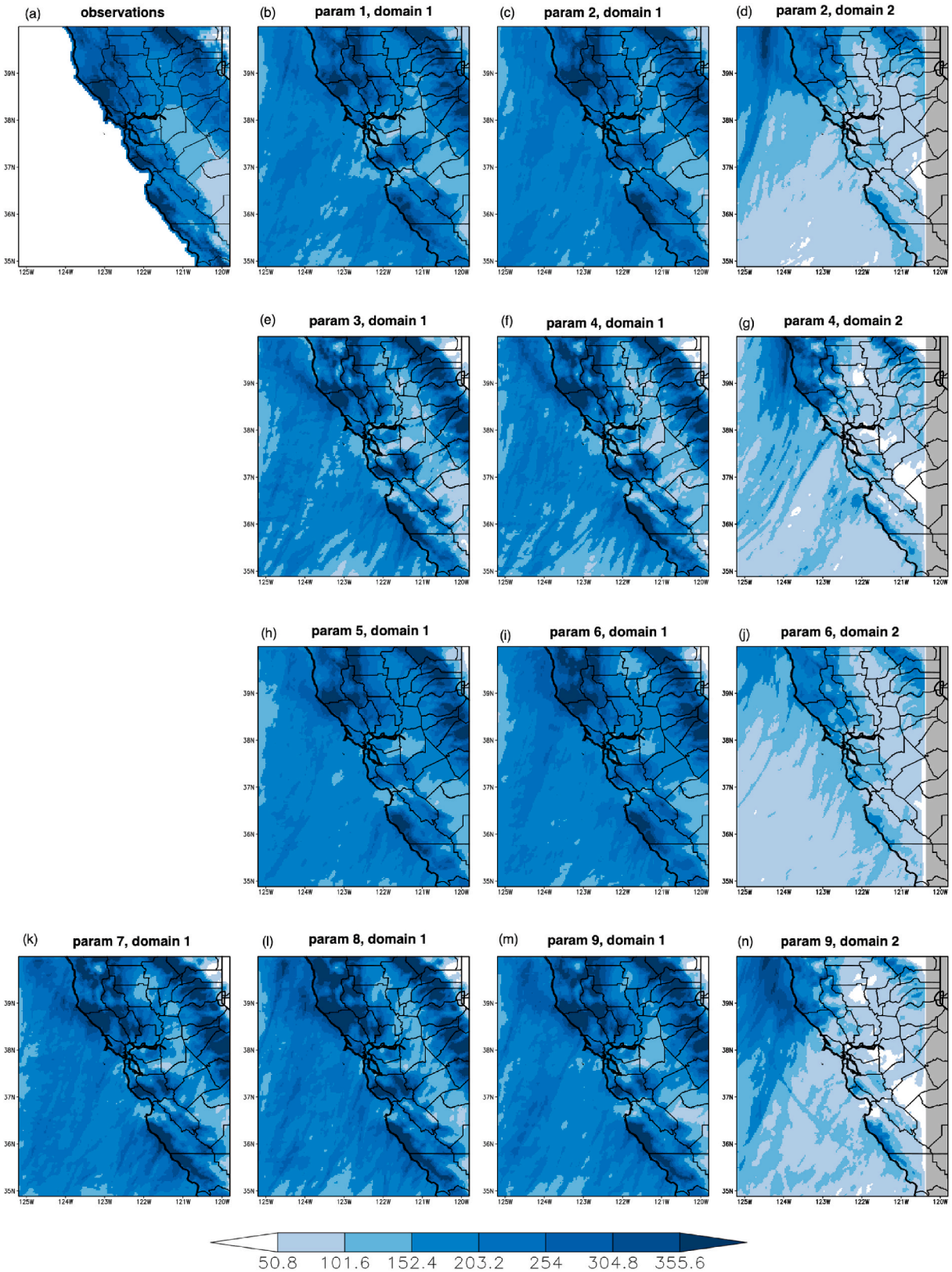

Fig. 2. Storm-total precipitation (mm) for storm 4 from (a) gridMET observations and WRF historical simulations on the 3 km resolution domain from tests of parameterizations (param) as in Table 2 and domains in Fig. 1: (b) param 1, domain 1, (c) param 2, domain 1, (d), param 2, domain 2, (e) param 3, domain 1, (f) param 4, domain 1, (g) param 4, domain 2, (h) param 5, domain 1, (i) param 6, domain 1, (j) param 6, domain 2, (k), param 7, domain 1, (l) param 8, domain 1, (m) param 9, domain 1, and (n) param 9, domain 2. Grey shading indicates no data.

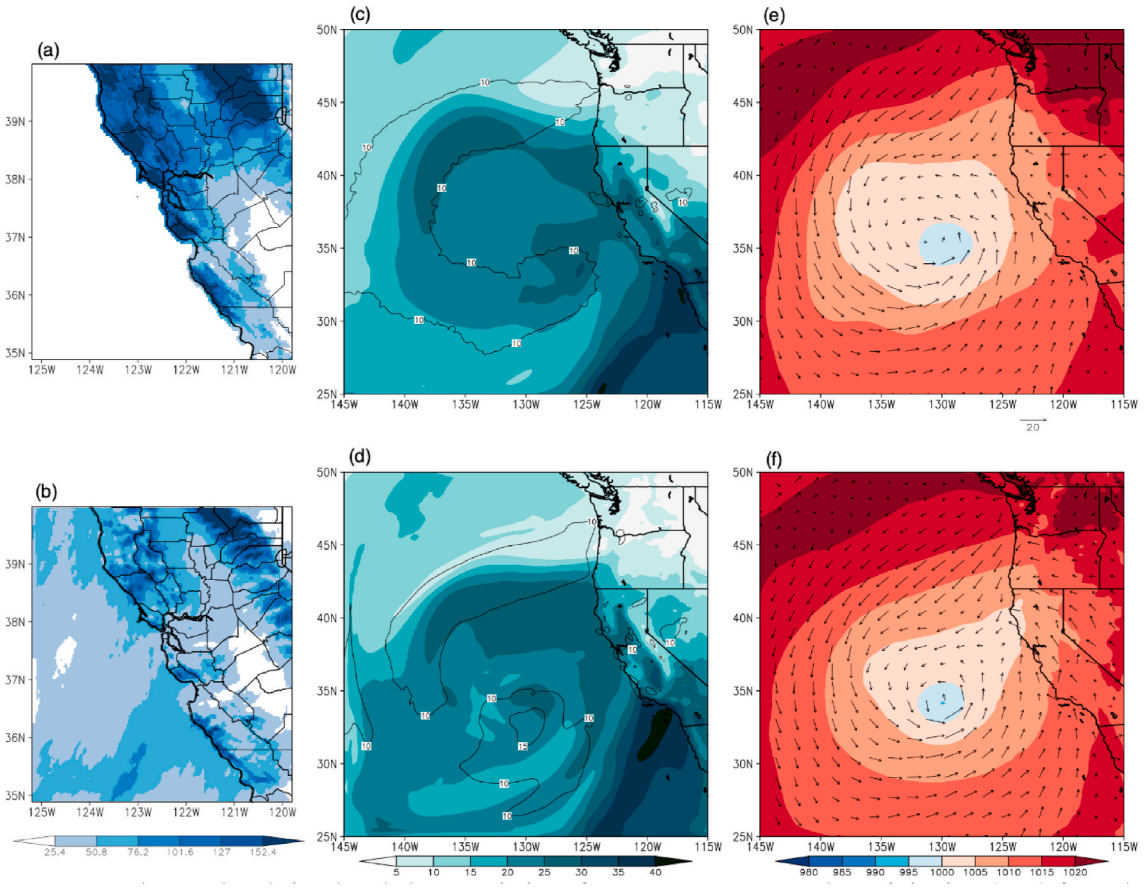

Fig. 3. Observed and simulated characteristics of storm 1a. Storm total precipitation (mm) from the (a) gridMET observations and (b) ensemble mean of the historical simulations on the 3 km resolution domain. Precipitable water (mm; shaded) and wind speed at 10-m (m/s; contour) from the (c) NARR and (d) ensemble mean of the historical simulations on the 27 km resolution domain. Wind speed contour interval is 5 m/s starting at 10 m/s. Sea-level pressure (mb; shaded) and 10-m wind (m/s; vectors) from the (c) NARR and (d) ensemble mean of the historical simulations on the 27 km resolution domain. Storm total precipitation is calculated over 00z 1 December - 00z December 7, 2014. Precipitable water, sea-level pressure, and 10-m wind are shown at the peak of the event, 00z December 3, 2014.

constraints (e.g., Allen and Ingram 2002; Held and Soden 2006). On the other hand, extreme precipitation at daily and hourly timescales typically scales at or above the CC rate of 6–7% per ^{o}C for significant amounts of warming (Kharin et al., 2013). For example, the scaling for hourly extreme precipitation (high percentiles) is double the CC rate in station observations over Hong Kong, the Netherlands, Belgium, and Switzerland for daily mean temperatures of at least 14 °C (Lenderink and van Meijgaard 2008, 2010; Lenderink et al., 2011). However, a global analysis of in-situ data reveals that CC scaling applies to daily extreme precipitation in only some regions, with CC scaling typical for sub-daily precipitation extremes (Utsumi et al., 2011). At the hourly scale, extreme precipitation from global rain gauge data follows at least CC scaling at a regional scale, with super-CC often found at the gauge-level (Ali et al., 2021.) Other studies found a temperature dependence of precipitation scaling, with extreme sub-daily precipitation scaling at CC for temperatures between 20°C-26°C, but decreasing for warmer temperatures, in station observations over Australia (Hardwick Jones et al., 2010). Precipitation scaling conditional on temperature has been termed "apparent scaling" (Fowler et al., 2021) and tends to indicate super CC scaling for sub-daily extremes within some temperature ranges (Westra et al., 2014), however scaling with temperature near the time of precipitation occurrence is not a reliable predictor for future changes in precipitation extremes in a climate model simulation (Sun et al., 2021). Precipitation scaling has also been investigated in climate model simulations, with extreme daily precipitation scaling at the CC rate (Allen and Ingram 2002), particularly in the mid-latitudes (Pall et al., 2007). Daily and hourly extreme precipitation exhibit scaling at the CC rate in convection-permitting climate model simulations (Ban et al., 2015), whereas 3-hourly extreme precipitation scaling exceeds CC in other model simulations (Wood and Ludwig 2020). The large variations in observed and simulated precipitation scaling rate have been linked with whether the environment is moist and energy-limited or dry and moisture limited (Prein et al., 2017).

In addition to dependence on precipitation frequency, data source (i.e., observations or models), and temperature, precipitation scaling can depend on storm type. Stratiform precipitation generally scales with CC, whereas convective precipitation scaling can exceed CC in radar and rain gauge data over Germany (Berg et al., 2013). Similarly, the intensity of extreme precipitation events increases at CC for non-convective events and above CC for convective events, identified as occurring without and with lightning, respectively, in station observations over Switzerland (Molnar et al., 2015). Finally, and of particular relevance to this study, the intensity of extreme precipitation events associated with AR type storms lasting longer than 10 h exceeds CC scaling in station data over Japan (Hatsuzuka et al., 2021), whereas the atmospheric moisture of ARs scales at about CC in historical observations (Algarra et al., 2020) and simulations of future climate (Zhao 2020). Altogether, previous studies on the scaling of extreme precipitation with temperature paint an uncertain picture of the magnitude of extreme precipitation change in a future warmer climate, highlighting the need for research that focuses on the storm type and precipitation timescale of interest.

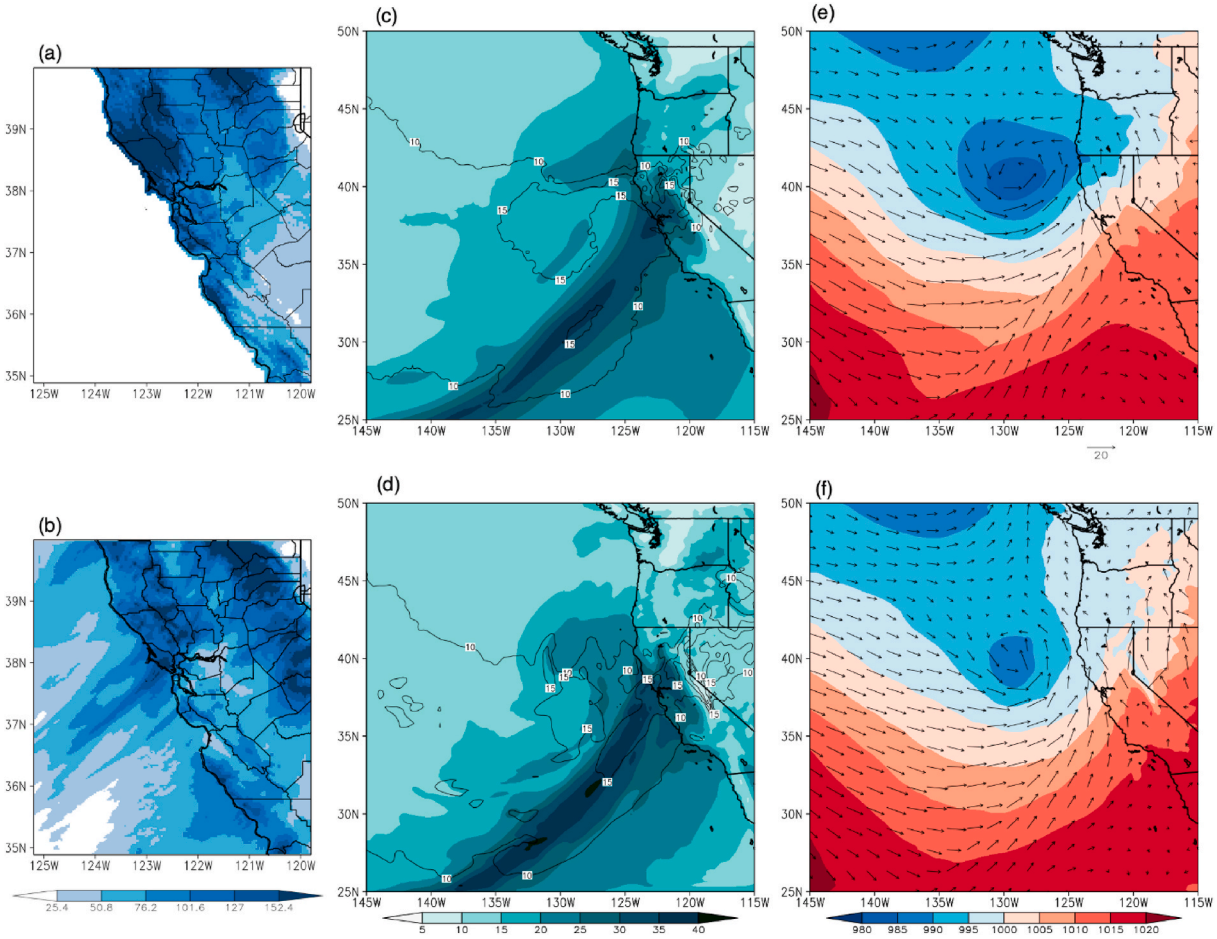

Fig. 4. Similar to Fig. 3, but for storm 1b. Storm total precipitation is calculated over 00z 10 December - 00z December 13, 2014. Precipitable water, sea-level pressure, and 10-m wind are shown at the peak of the event, 12z December 11, 2014.

The second reason that future precipitation projections are uncertain is that many climate model simulations have difficulty reproducing extreme precipitation rates. The typical horizontal resolution for global climate model simulations is currently 1°-2.5°, with 0.25° considered relatively high-resolution. Nonetheless, even the current relatively high-resolution global climate models struggle to simulate the extreme precipitation rates observed at the spatial scales relevant for decision making (e.g., Wehner et al., 2014; 2020), as the grid spacing is too coarse to directly resolve convective processes.

The purpose of this study is to quantify future changes in the magnitude of extreme precipitation events over the San Francisco Bay Area (hereafter the Bay Area) and to understand the scaling of precipitation with temperature in AR and ETC events. In order to better simulate extreme precipitation magnitudes and to eliminate the uncertainty associated with the use of climate model parameterization of convection, we performed hindcasts of selected historical storms with a horizontal resolution of 3 km (~0.027°) over the Bay Area and simulations with imposed future warming (Schär et al., 1996). This research provides very high-resolution extreme precipitation projections using state-of-the-art climate modeling methods along with a physical understanding of the future changes in ARs and ETCs. It is motivated by the needs of the project's stakeholder working group, which is composed of members from the City and County of San Francisco (CCSF), and led by the San Francisco Public Utilities Commission (SFPUC), with support from the San Francisco International Airport (SFO), the Office of Resilience and Capital Planning, and the Port of San Francisco.

2. Data and methods

2.1. Convection-permitting regional climate model simulations

Regional climate model simulations were performed with the Weather Research and Forecasting (WRF) model version 3.8.1 (Skamarock and Klemp 2008), which is developed and maintained by the National Center for Atmospheric Research (NCAR). A regional climate model is best suited for this study because it allows computational resources to be used for higher-resolution focused over the region of interest, namely the Bay Area. The model is configured using one-way nested domains, so that in addition to simulating the Bay Area at high-resolution, ARs and ETCs that are approaching land from the North Pacific Ocean can also be simulated, albeit at a coarser but sufficient resolution. The domains include a 27 km resolution parent domain, a 9 km nested domain, and a 3 km innermost domain (Fig. 1a). High-resolution is crucial for this study, as coarse-resolution (~100–250 km) climate models poorly represent the observed extreme precipitation characteristic of impactful Bay Area storms (Wehner et al., 2014; 2020). WRF is configured with 44 levels in the vertical. Model output for 3D variables is saved every 3-h, and selected surface variables are saved at a frequency of 5 min.

The simulations are based on five historically-impactful extreme precipitation events ranging from several days to over a week in duration (Table 1). The events were selected with input from the stakeholder working group. In particular, stakeholders from the CCSF completed a survey to provide input on past storm events that impacted their agencies by causing flooding, physical damage, or operational

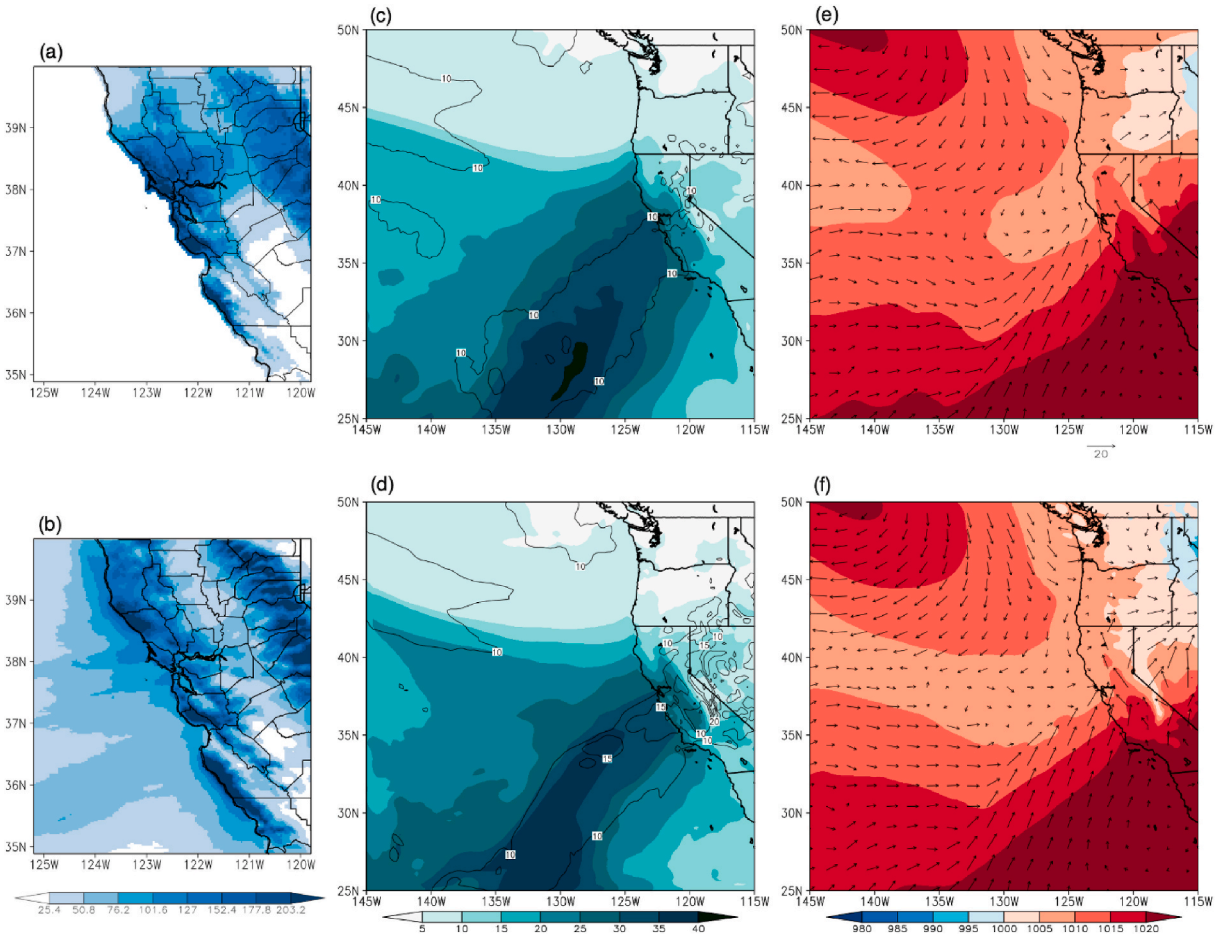

Fig. 5. Similar to Fig. 3, but for storm 2. Storm total precipitation is calculated over 00z 2 January - 00z January 6, 1982. Precipitable water, sea-level pressure, and 10-m wind are shown at the peak of the event, 18z January 4, 1982.

challenges. The storm events identified using the survey focused on recent history (2004 to present); however, some of the most severe events in the Bay Area occurred in the 1980s and 1990s. Therefore, we performed a systematic analysis of the observational record to identify storm events that were extreme in terms of storm-total precipitation, 1-h, 3-h, 12-h, and 24-h maximum precipitation, storm duration, hourly wind speed and gusts, and sea-level pressure. We note that of the 14 candidate storm events, 13 of the events occurred with an AR (and sometimes an ETC). Due to the high computational cost of the simulations, we were unable to include all impactful events in this study. However, by selecting storm events with different characteristics, (i.e., AR only or AR with an ETC), we attempt to represent the typical types of extreme precipitation events that impact the Bay Area.

Five events were selected, as this was the greatest number of events that could be simulated with the available supercomputing resources, while meeting simulation design requirements (e.g., 3 km resolution over the Bay Area and a multi-member ensemble). Note that storm 1 consisted of two distinct periods of precipitation with a break in between, therefore separate simulations of this event were performed for the two precipitation periods, named storm 1a and storm 1b, to allow for an improved quality hindcast of the latter portion of the event enabled by reinitializing the model. Initial conditions, lateral boundary conditions, and sea-surface temperatures (SSTs) were prescribed from the North American Regional Reanalysis (NARR; Mesinger et al., 2006). The quality of the input data influences the ability of the climate model to represent the observed historical storm events, with higher spatial resolution and temporal frequency tending to improve the simulations. For this reason, the NARR was chosen for its relatively high spatial resolution of 32 km × 32 km and a temporal frequency of 3-h and for its spatial coverage over the parent domain region. Model initialization is a few days before the start of precipitation over the Bay Area (Table 1) to permit the model to adjust to climate change perturbations described below. We performed a 10-member ensemble of each simulation to provide a range for future precipitation estimates, allowing us to evaluate statistical significance by comparing the climate change signal to noise associated with internal atmospheric variability. Each ensemble member was generated by initializing the simulation at different times at three-hourly intervals (e,g., 00z, 03z, 06z; Table 1). We found that a 10-member ensemble is suitable for this study, as discussed in section 3.2.

For each of the five storm events, we performed three sets of simulations for different climate states including the historical period (i.e., the time in which the storm event actually occurred) and two future periods (2040–2060 and 2080–2100) under the Representative Concentration Pathway (RCP) 8.5 greenhouse gas emissions scenario (Meinshausen et al., 2011). The purpose of the simulations is to estimate how climate change could influence precipitation events similar to known historically impactful events. We emphasize that it is not necessary for the historical simulation hindcasts to precisely reproduce the timing and location of the events. Specifically, we cannot expect the historical simulations to better reproduce observations than a weather forecast model would. For example, it is reasonable to expect that a weather forecast model would predict that a storm will occur in a general region such as the Bay Area, but unreasonable to expect that a weather forecast model would predict storm-total precipitation at a specific location within a few mm (tenths of inches).

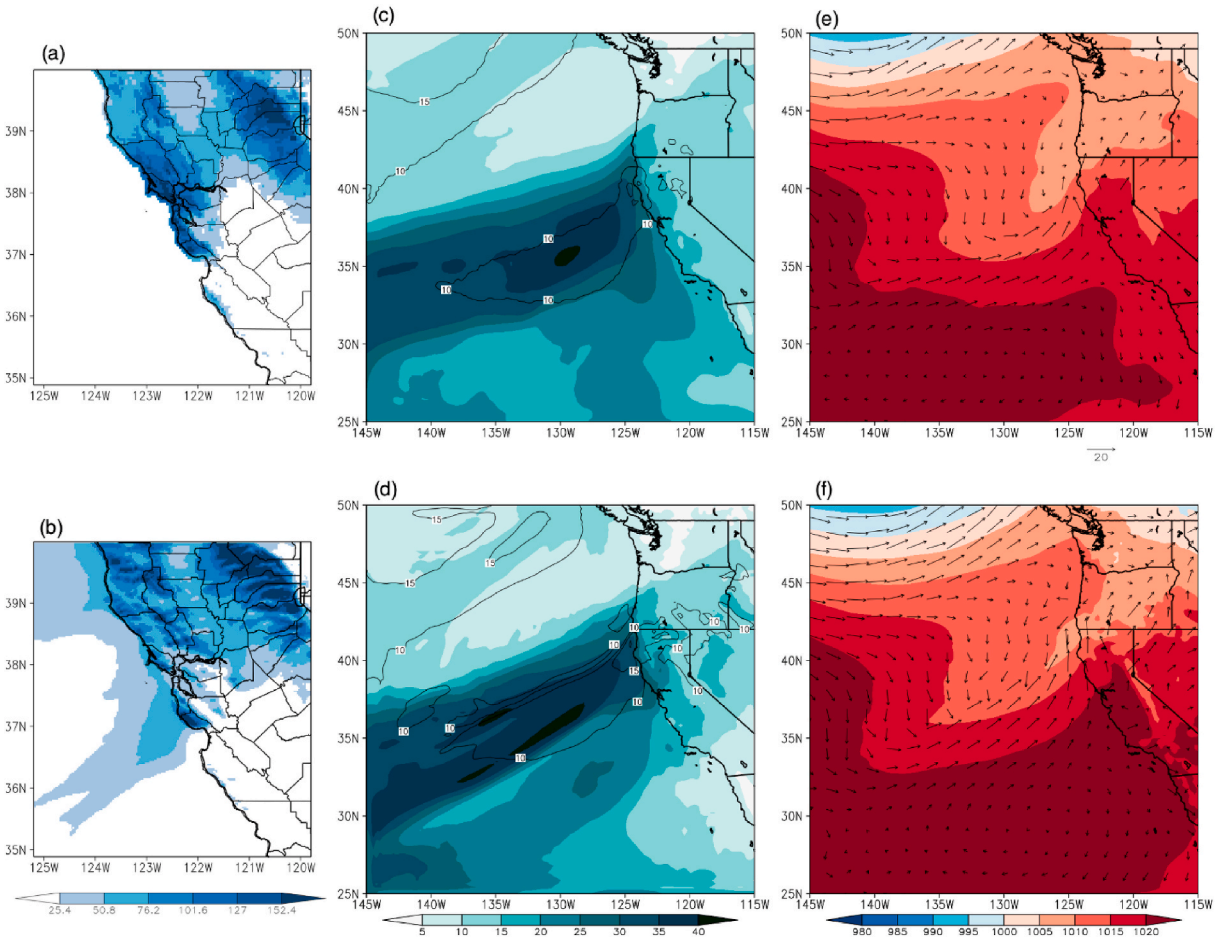

Fig. 6. Similar to Fig. 3, but for storm 3. Storm total precipitation is calculated over 00z 3 November - 00z November 8, 1994. Precipitable water, sea-level pressure, and 10-m wind are shown at the peak of the event, 00z November 5, 1994.

Initial conditions, lateral boundary conditions, and SSTs for the future simulations were based on those from the historical simulations, with adjustments to impose the thermodynamic component of anthropogenic climate change (e.g., Schär et al., 1996; Patricola and Cook 2010, 2013). Dynamic variables remained unchanged, which is reasonable for this hypothetical event-based approach that focuses on future changes in precipitation magnitude, however we note that changes in dynamic variables (e.g., the jet stream) should be considered for studies that investigate future changes in AR and/or ETC frequency in long-term climate simulations. The future initial and boundary condition changes were based on simulations from the CESM large ensemble (Kay et al., 2015). The climate change perturbations for the RCP8.5 experiment for the mid-21st century (2050) and late-21st century (2100) for storm 1 were calculated as the December climatology of 2040–2060 and 2080–2100, respectively, from the RCP8.5 simulation minus the 1980–2000 December climatology from the historical simulation. This perturbation was then added to the historical boundary conditions. The perturbations for all other storms were calculated in the same way, but for the month in which the event occurred. This methodology has been used to study anthropogenic influences on AR, tropical cyclone, tornadic storm, and flood events, as well as seasonal snowpack and associated runoff (e.g., Rasmussen et al., 2011; Lackmann 2015; Takayabu et al., 2015; Ito et al., 2016; Nakamura et al., 2016; Pall et al., 2017; Dominguez et al., 2018; Patricola and Wehner 2018; Gutmann, 2018; Wehner et al., 2019; Bercos-Hickey et al. 2021; Ikeda et al., 2021, and others). Using the climate perturbation that corresponds to the month of the storm event is a good balance between precision and implementation. Greenhouse gas concentrations including CO_2, CH_4, N_2O, CFC-11, CFC-12 and CCl_4, were prescribed according to Tsutsumi et al. (2009) and Bullister (2015).

2.2. Regional climate model optimization

We performed tests on two known aspects of regional climate model configuration that can influence the outcome of the simulation, namely physical parameterizations and model domain. The purpose of the model testing was to select a model configuration that is optimized to provide the best quality data to assess future change in Bay Area extreme precipitation.

There are many parameterization options to choose from in WRF. The primary variables of interest for the stakeholder working group are precipitation and 10-m wind, therefore we tested parameterizations most relevant for these variables, specifically microphysics and planetary boundary layer. Convection parameterization is also relevant for precipitation, however testing was not performed because the parameterization was not needed at the convection-permitting resolution of the 3 km domain over the Bay Area, and due to limited supercomputing resources. We note that nested domains that explicitly resolve convection can be sensitive to the convective parameterization choice in outer domains that do not resolve convection due to the influence on vertical temperature and humidity profiles (Di Luca et al., 2021). The parameterizations for atmospheric radiation and land-surface model were selected based on previous experience simulating the climate of California (e.g. Patricola et al., 2020) and included the Rapid Radiative Transfer Model for General Circulation Models (RRTMG) shortwave and longwave radiation scheme (Mlawer et al., 1997), the Noah Land

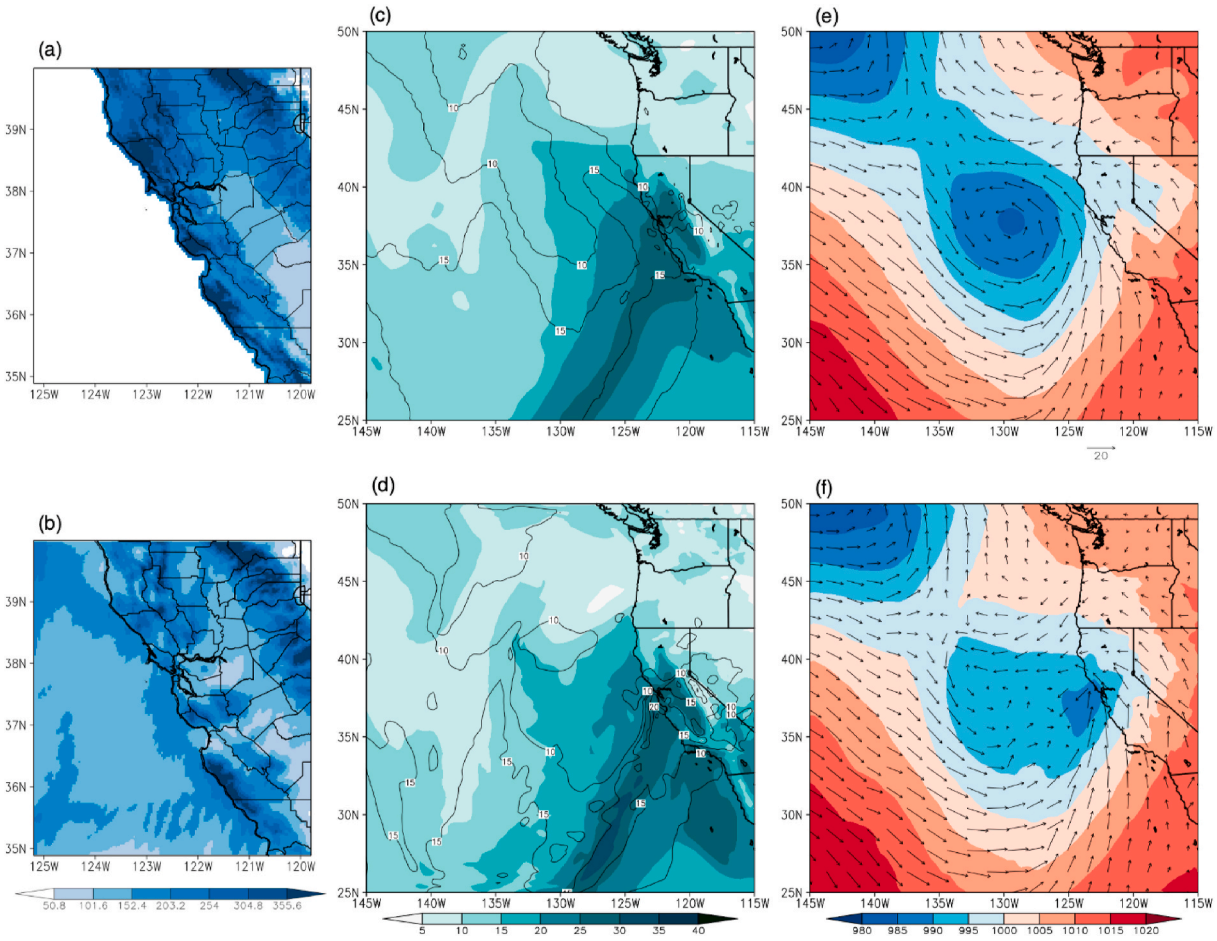

Fig. 7. Similar to Fig. 3, but for storm 4. Storm total precipitation is calculated over 00z 30 January - 00z February 9, 1998. Precipitable water, sea-level pressure, and 10-m wind are shown at the peak of the event, 00z February 3, 1998.

Surface Model (Chen and Dudhia 2001), and the Kain-Fritsch convective parameterization (Kain and Fritsch 1990; Kain 2004) for the outer 27 km domain.

We performed simulations to test nine sets of parameterizations (Table 2) on two model domains (Fig. 1). The test simulations were run for storm event 4 because it was characterized by the greatest storm-total precipitation of the selected events. We compared simulated precipitation with observations from the daily 4 km resolution gridMET dataset (Abatzoglou 2013). All of the test simulations on domain 1 are able to reproduce relatively greater storm-total precipitation observed over regions of higher elevation (Fig. 2). Storm-total precipitation was calculated over the storm event shown in Table 1 and averaged over the Bay Area region shown in Fig. 9a. The simulated differences among the parameterization options are relatively small (Fig. 2), and any of the options would be suitable for this study. Parameterization sets 8 and 9 slightly better represent the magnitude of storm-total rainfall area-averaged over the Bay Area compared with the other options. Therefore, we selected parameterization set 9 for the full set of model experiments (i.e., the Yonsei University (YSU) planetary boundary layer scheme, the WRF Single-Moment 6-Class Microphysics (WSM6) scheme, and the other parameterizations discussed above).

Regional climate models require the user to choose one or more geographic regions for simulation, called "domains." A configuration with multiple domains within each other is called a "nested domain." Each domain has a corresponding model resolution. In the nested domain configuration, the resolution is coarsest on the largest outer domain and is finer by a factor of three for each nested inner domain. We tested the climate model using two different domain configurations, described below. Both domains use 3 km resolution over the Bay Area. The two domain configurations are different in how geographically extensive the outer 27 km domain is.

The nested domains are updated at the lateral boundaries at a frequency corresponding to the model time step of the coarser surrounding domain. For example, the lateral boundaries for the 9 km domain are updated at a frequency of 90 s, which corresponds to the 27 km domain time step. Likewise, the lateral boundaries for the 3 km domain are updated at a frequency of 30 s, which corresponds to the 9 km domain time step. The variables updated at the lateral boundaries of the nested domains include the variables prescribed on the outermost domain by the NARR reanalysis, such as temperature, zonal and meridional winds, humidity, and geopotential height, as well as hydrometeor variables calculated by the WRF model.

The rationale for testing different domain configurations is that the simulation can depend on how far the edges of the outer domain are from the region of interest, in this case the Bay Area. Regional climate models need information about the observed state of the atmosphere at the domain edges. A smaller outer model domain with edges closer to the Bay Area means the observational products more tightly constrain the simulation, which tends to produce a model simulation that more closely represents what was observed. A model simulation that represents the observed storms well is desirable, however the primary purpose of the simulations is to estimate how the storms respond to climate change, therefore our optimization process focuses not on producing a "perfect" hindcast (which would be an unrealistic expectation for the model), but instead on producing a reasonable hindcast within a simulation design that permits climate change experiments. If the outer

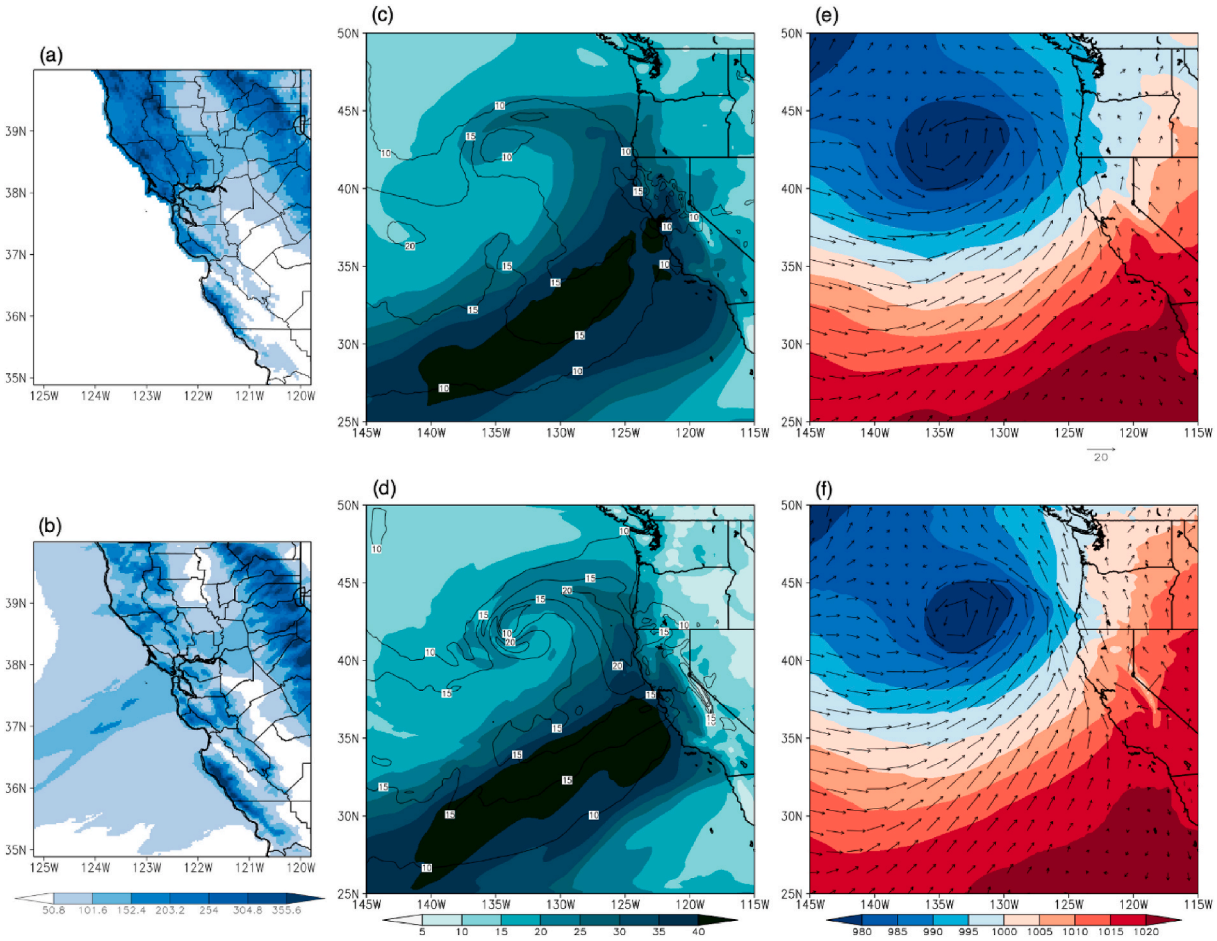

Fig. 8. Similar to Fig. 3, but for storm 5. Storm total precipitation is calculated over 00z 9 December - 00z December 14, 1995. Precipitable water, sea-level pressure, and 10-m wind are shown at the peak of the event, 06z December 12, 1995.

domain is too small, the climate model simulation will be over-constrained and may not capture the climate change response well. For example, if an AR is approaching, the outer domain should be extensive enough that it contains the AR and permits it to respond to the climate change imposed on the model. On the other hand, an outer domain that is too large may not reproduce an observed storm event as well.

We tested two domain configurations, which represent medium and large sized outer domains, domain 1 (Fig. 1a) and domain 2 (Fig. 1b) respectively. In addition to the parameterization testing for domain 1 described above, we tested a subset of parameterization options (sets 2, 4, 6, and 9) for domain 2. Regardless of the parameterization options selected, the regional model better simulates the storm-total rainfall for domain 1 compared with domain 2 (Fig. 2). The storm-total rainfall for domain 2 is substantially less than observed, indicating that an outer domain of this size is too large for this study. Therefore, we selected domain 1 to perform the full set of model experiments, as it contains sufficient space for ARs and ETCs to develop as they approach the California coast and reproduces observed precipitation reasonably well, as described in the following section.

3. Results

3.1. Historical storm events

For each of the historical events, we identified the type of storm (i.e., atmospheric river and/or extratropical cyclone), so that we can determine any dependence of future changes in precipitation on storm type. In addition, we compared the observed and ensemble-mean simulated storm-total precipitation, sea-level pressure, and precipitable water to evaluate how well the model reproduced each event. Historical storm events that were reasonably reproduced by the model may have less uncertainty associated with their corresponding projected future change in precipitation, whereas events that were more difficult for the model to represent may inspire less confidence in their future projections.

The historical storm events considered in this study are characterized by two main types of synoptic conditions, namely, an AR only or an AR accompanied by an ETC. These are the primary types of storms that deliver extreme precipitation to the Bay Area in the historical climate, and are expected to continue as such into the future (e.g., Gershunov et al., 2019). To identify the type of storm event, we examined sea-level pressure, precipitable water, and 10-m winds throughout the evolution of each storm, with these variables shown at the peak of the event (i.e., approximately the time of strongest precipitation observed over the Bay Area) in Figs. 3–8. To summarize our findings, the historical simulations reproduced the observed synoptic conditions (AR and ETC location and magnitude) and spatial pattern of storm-total precipitation very well for all storm events, and underestimated, but still reasonably simulated, the magnitude of storm-total precipitation (i.e., simulated storm-total precipitation is within about half to double the observed rate, and simulated AR and ETC timing and location is close to observed). Storm events 1, 4, and 5 were characterized by an AR accompanied by an ETC, whereas storm events 2 and 3 were characterized by only an AR. A detailed description of each storm event follows.

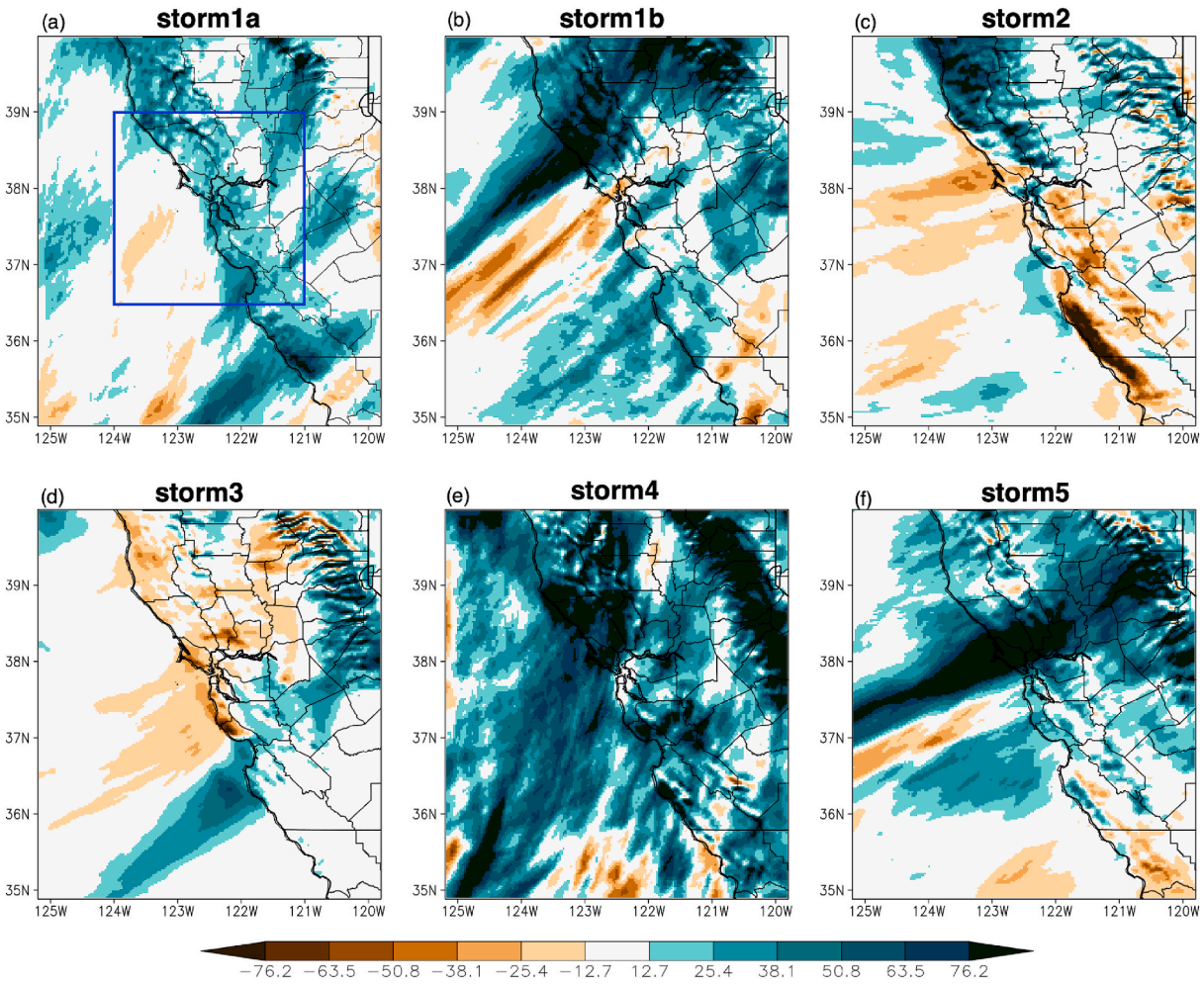

Fig. 9. Future change in storm total precipitation (mm) from the ensemble mean of the 2100 minus historical simulations on the 3 km resolution domain for (a) storm 1a, (b) storm 1b, (c) storm 2, (d) storm 3, (e) storm 4, and (f) storm 5. Storm total precipitation is calculated over (a) 00z 1 Dec - 00z Dec 7, 2014, (b) 00z 10 Dec - 00z Dec 13, 2014, (c) 00z 2 Jan - 00z Jan 6, 1982, (d) 00z 3 Nov - 00z Nov 8, 1994, (e) 00z 30 Jan - 00z Feb 9, 1998, and (f) 00z 9 Dec - 00z Dec 14, 1995, as in Figs. 3–8. The blue box in (a) shows the averaging region used in the calculations for Table 3. (For interpretation of the references to color in this figure legend, the reader is referred to the Web version of this article.)

3.1.1. Storm 1

Storm 1 consisted of two distinct periods of Bay Area precipitation over December 2–6, 2014 (storm 1a) and December 11–12, 2014 (storm 1b), with about a five-day break in between. Storm 1a was characterized by precipitation reaching up to, and in some places over, 6 inches (~152 mm) according to the gridMET observations (Fig. 3a). The ensemble-mean historical simulation produced storm-totals that are weaker than observed, but reproduced the spatial pattern of precipitation reasonably well with greater amounts over high-terrain regions (Fig. 3b). Precipitable water was moderate over the Bay Area and offshore region, with a landfalling AR further south over southern California and northwestern Mexico (Fig. 3c), and a weak offshore ETC (Fig. 3e), both of which were reproduced well in the historical simulation (Fig. 3d and f).

Like storm 1a, storm 1b was characterized by storm-total precipitation reaching over 6 inches, although the duration of rainfall was shorter (Fig. 4a). The historical simulation reproduced the precipitation magnitude relatively well (Fig. 4b), especially compared with storm 1a. The ETC that was offshore on December 3, 2014 intensified and moved northeastward toward the coast of northern California and Oregon in both the NARR (Fig. 4e) and historical simulation (Fig. 4f). In addition, the precipitable water and 10-m winds indicate a clearly defined AR making landfall directly over the Bay Area and oriented from southwest to northeast (Fig. 4c and d).

3.1.2. Storm 2

Storm 2 was a relatively short duration but strong magnitude event, with up to 8 inches (~203 mm) of precipitation falling over the Bay Area from January 3–5, 1982 (Fig. 5a), which was reproduced well by the historical simulation (Fig. 5b). Unlike storm 1, storm 2 was characterized by only an AR oriented southwest to northeast (Fig. 5c and d), without an accompanying ETC (Fig. 5e and f). The magnitude of precipitable water was comparable between storm 2 (Fig. 5c) and storm 1b (Fig. 4c).

3.1.3. Storm 3

Storm 3 produced up to 6 inches of precipitation over the Bay Area over November 4–7, 1994 (Fig. 6a), which was simulated with a weaker magnitude in the historical hindcast (Fig. 6b). Like storm 2, this event was characterized by only an AR (Fig. 6c) without an accompanying ETC (Fig. 6e). The AR was oriented from west-southwest to east-northeast with strong precipitable water. The historical simulation reproduced the AR location and magnitude, as well as the lack of an ETC, very well (Fig. 6d and f).

3.1.4. Storm 4

Storm 4 was characterized by the greatest magnitude of storm-total precipitation and longest duration of the events considered, with over 14 inches (~356 mm) falling over the Bay Area between January 31 -

Table 3
Percent change in storm-total precipitation between the future and historical simulations ((future minus historical)/historical) on the 3 km and 27 km (in parentheses) domains, the theoretical change if precipitation were to scale at the CC rate (6.5% per °C, where temperature is the average 2-m temperature over ocean only in the offshore region of 30°N-40°N and 130°W-120°W), the ratio of the simulated precipitation scaling to the CC scaling rate, and positive vertical velocity at 500 hPa. Simulated changes in storm-total precipitation that are statistically significant ($p = 0.01$; two-tailed *t*-test) are bold. Storm-total precipitation and vertical velocity are calculated over the same days as in Fig. 9 and are averaged over land only over approximately the San Francisco Bay Area (36.5°N-39°N and 124°W-121°W, i.e., the region in the blue box in Fig. 9a).

Storm total precipitation	Storm 1a	Storm 1b	Storm 2	Storm 3	Storm 4	Storm 5
Storm type	AR & ETC	AR & ETC	AR only	AR only	AR & ETC	AR & ETC
2050 WRF	17% (25%)	11% (12%)	5% (4%)	−8% (−10%)	7% (9%)	15% (12%)
2100 WRF	**37% (44%)**	**26% (19%)**	**2%** (0%)	**−11% (-15%)**	**31% (35%)**	**34% (22%)**
2050 CC	12%	12%	11%	12%	10%	12%
2100 CC	24%	25%	23%	25%	21%	25%
2050 WRF/CC	1.4	0.9	0.4	−0.7	0.7	1.2
2100 WRF/CC	1.5	1.1	0.1	−0.4	1.4	1.4
Precipitable water	**Storm 1a**	**Storm 1b**	**Storm 2**	**Storm 3**	**Storm 4**	**Storm 5**
2050 WRF/CC	1.4	1.4	1.2	1.7	1.2	1.5
2100 WRF/CC	1.5	1.5	1.2	1.7	1.5	1.6
IVT	**Storm 1a**	**Storm 1b**	**Storm 2**	**Storm 3**	**Storm 4**	**Storm 5**
2050 WRF/CC	1.2	1.5	1.2	1.4	1.2	1.7
2100 WRF/CC	1.5	1.6	1.3	1.6	1.7	1.8
500 hPa vertical velocity	**Storm 1a**	**Storm 1b**	**Storm 2**	**Storm 3**	**Storm 4**	**Storm 5**
2050 WRF	0.5%	5.9%	−0.1%	−1.9%	3.5%	4.3%
2100 WRF	7.3%	18.3%	−4.3%	−1.5%	10.6%	8.3%

February 8, 1998 (Fig. 7a). It occurred during a strong El Niño event, which often drives wetter than average winter precipitation over California (e.g., Patricola et al., 2020). The historical simulation reproduced the storm-total precipitation reasonably well (Fig. 7b), albeit with a weaker magnitude than observed. This event was characterized by an AR oriented from the southwest to northeast accompanied by an ETC (Fig. 7c–f).

3.1.5. *Storm 5*

Storm 5 delivered up to 8–10 inches (~203–254 mm) of precipitation over parts of the Bay Area during December 10–13, 1995 (Fig. 8a). As with several other storm events, the historical simulation reproduced

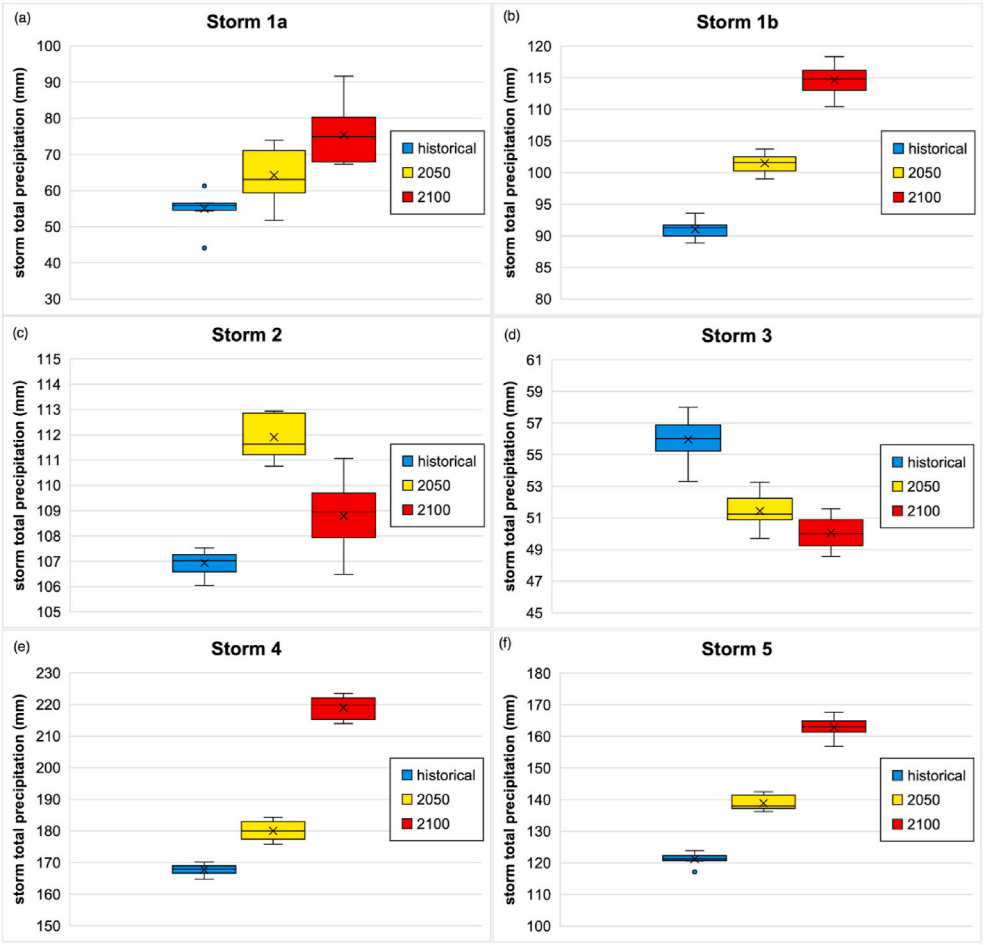

Fig. 10. Boxplots of storm-total precipitation (mm) averaged over the San Francisco Bay Area region (Fig. 9a) from the 10-member ensemble of the historical (blue), 2050 (yellow), and 2100 (red) simulations from (a) storm 1a, (b) storm1b, (c) storm 2, (d) storm 3, (e) storm 4, and (f) storm 5. The x denotes the ensemble-average, and the lines that make up the box denote the 25th, 50th, and 75th percentiles. (For interpretation of the references to color in this figure legend, the reader is referred to the Web version of this article.)

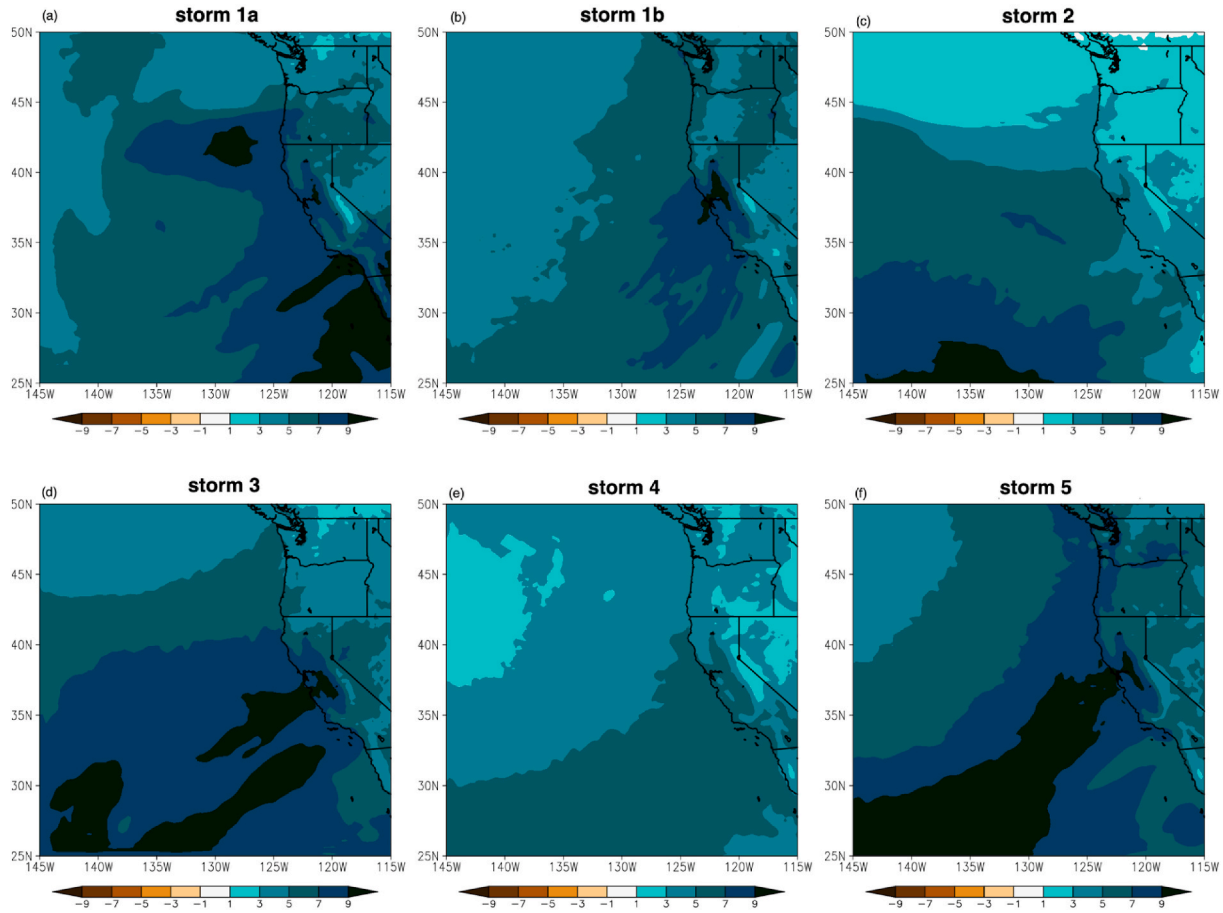

Fig. 11. Future change in precipitable water (mm) from the ensemble mean of the 2100 minus historical simulations on the 27 km resolution domain for (a) storm 1a, (b) storm 1b, (c) storm 2, (d) storm 3, (e) storm 4, (f) storm 5. Precipitable water for each event is calculated over the same days as in Fig. 9.

the spatial pattern of precipitation well, with a reasonable but weaker than observed magnitude (Fig. 8b). Like storm 1 and 4, storm 5 was characterized by an AR accompanied by an ETC (Fig. 8c and e), both of which were the strongest of the events considered and were reproduced well in the historical simulation (Fig. 8d and f).

3.2. *Future changes in precipitation*

Having identified the storm type for each historical event in the previous section, we now quantify future changes in storm-total precipitation, calculate the simulated precipitation scaling and compare it with the theoretical CC scaling rate, and analyze any dependence on storm type. Maps of the projected future changes (2100 minus historical) in ensemble-mean storm-total precipitation from the 3 km model domain are shown in Fig. 9, with percentage changes ((future - historical)/historical) for the 2100 and 2050 simulations averaged over the Bay Area (blue box in Fig. 9a) from both the 3 km and 27 km model domains shown in Table 3. We calculated the percentage changes in storm total precipitation for each storm event by (1) calculating the total precipitation over the storm life time for each ensemble member (listed under “event dates” in Tables 1) and (2) then taking the area-average of this quantity over the San Francisco Bay Area region shown in Fig. 9a over land only, (3) then computing the 10-member ensemble mean of this quantity, for each climate scenario, and finally (4) calculating the percentage change using these ensemble-mean quantities for ((future - historical)/historical). The calculation is performed with this order of operations so that the percentage change is appropriate, rather than calculating the percentage change for each ensemble member and then averaging them. We verified that any spatial shifts in the location of precipitation between the historical and future simulations for a given event were relatively small (i.e., confined within the Bay Area region of interest), therefore we are able to make a fair comparison between the storm events in the different climate states. The ensemble-mean storm-total precipitation from the 3 km model domain increases over the Bay Area from the historical to the 2100 simulations for storms characterized by an AR accompanied by an ETC (i.e., storms 1a, 1b, 4, and 5), whereas the precipitation change is a mix of increases and decreases for storms characterized by an AR only (i.e., storms 2 and 3) (Fig. 9 and Table 3). These changes correspond to statistically significant (1% level, two-tailed *t*-test) increases in Bay Area precipitation of 7–17% for 2050 relative to historical and 26–37% for 2100 relative to historical, for co-occurring AR and ETC events (Table 3). For AR-only events, Bay Area precipitation changes span zero, ranging from −8% to 5% for 2050 and -11%–2% for 2100 (Table 3). The magnitude of storm-total precipitation increases for events characterized by an AR accompanied by an ETC is similar to that projected by WRF simulations that downscaled simulated AR events from a global climate model (Huang et al., 2020).

We examined the ensemble spread in storm-total precipitation in the historical and future climate scenarios to verify that the ensemble size is sufficient using boxplots containing the storm-total precipitation for each ensemble member for a given climate scenario and storm event (Fig. 10). In the storms characterized by a co-occurring AR and ETC (Fig. 10 a-b, e-f), the range of simulated storm-total precipitation within an ensemble typically shows little-to-no overlap between climate scenarios, suggesting that the climate change signal is much greater than noise due to internal atmospheric variability within the ensemble. This analysis indicates that a 10-member ensemble is suitable for this study. Finally, the projected precipitation changes vary by about ± 12%

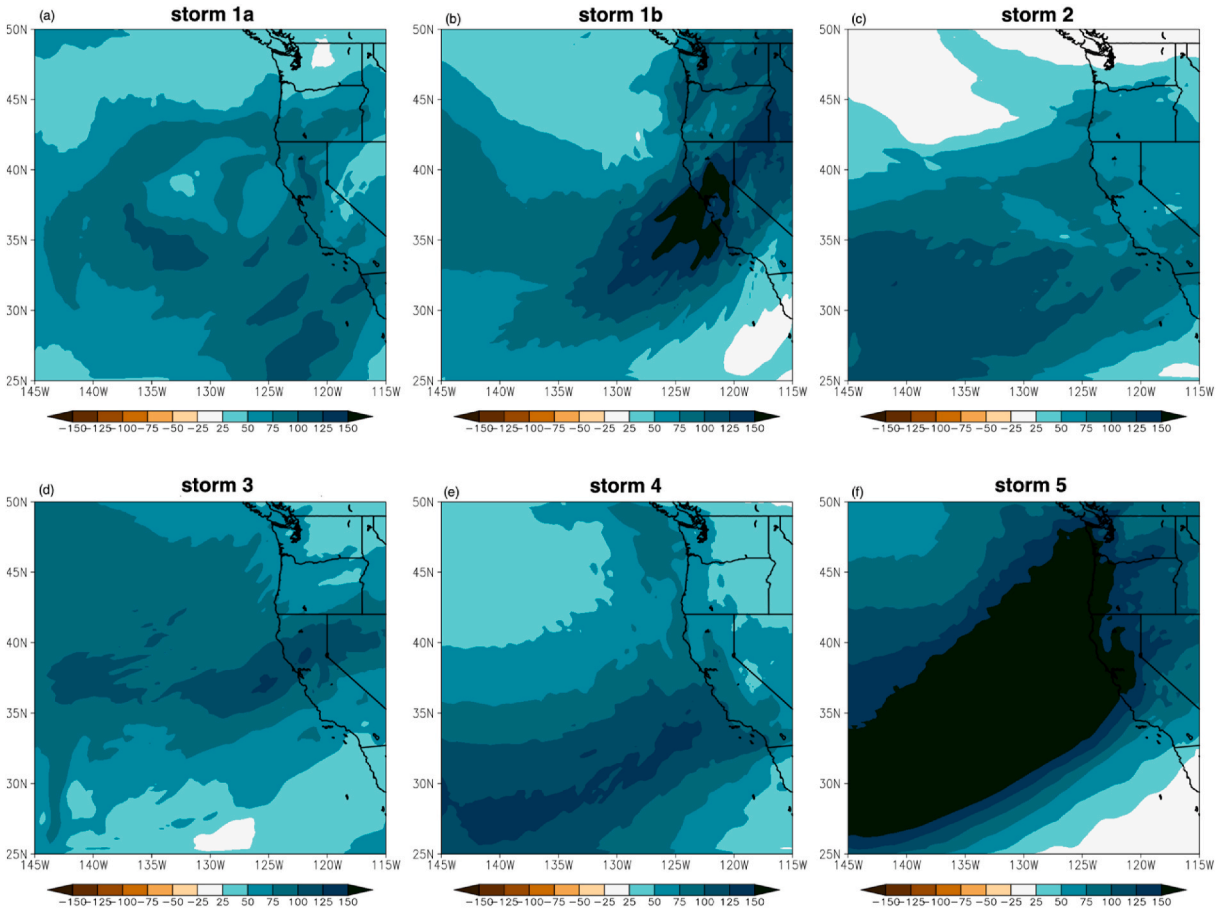

Fig. 12. Future change in IVT (km m^{-1} s^{-1}) from the ensemble mean of the 2100 minus historical simulations on the 27 km resolution domain for (a) storm 1a, (b) storm 1b, (c) storm 2, (d) storm 3, (e) storm 4, (f) storm 5. IVT for each event is calculated over the same days as in Fig. 9.

depending on model resolution, although the difference is not systematic (i.e., the 3 km resolution domain does not always simulate higher or lower changes relative to the 27 km resolution domain). For the remainder of the analysis, we focus on precipitation from the 3 km domain.

We next investigated the simulated precipitation scaling rate, that is, the percent change in future precipitation per °C of warming (Table 3). The magnitude of simulated temperature change was calculated using the average 2-m temperature over the ocean only in the region offshore from the Bay Area (30°N-40°N and 130°W-120°W) for the 2100 minus historical and the 2050 minus historical simulations, for each storm event. In addition, we used the corresponding simulated temperature change to estimate the hypothetical precipitation change according to the CC scaling rate of a 6.5% increase in precipitation per °C of temperature warming (Table 3). Finally, we calculated the ratio of simulated precipitation scaling to CC scaling to determine whether the simulated precipitation scaling is less than (ratio <1), approximately equal to (ratio equals 1), or exceeds (ratio >1) the CC scaling rate (Table 3).

The future Bay Area storm-total precipitation changes exhibit a strong dependence on storm type, with the caveat that the sample size includes five events. Focusing on the 2100 simulations, storms characterized by an AR accompanied by an ETC (i.e., storms 1, 4, and 5) exhibit precipitation scaling that exceeds the CC rate (1.1–1.5 times CC), whereas precipitation scaling is below CC or negative, indicating a decrease in precipitation, for storms 2 and 3, which were characterized by an AR only (Table 3). Our findings may be consistent with observed precipitation scaling rates for AR-type events in the historical climate, which were found to exceed CC (Hatsuzuka et al., 2021), although information is unavailable on whether the AR-type events were accompanied by an ETC. If our discovery that precipitation scaling with future warming exceeds the CC scaling rate for the storms characterized by an AR accompanied by an ETC generalizes to all such storms, there are important implications for projected future precipitation impacts, as the majority of observed AR events (82%) are associated with an ETC (Zhang et al., 2019).

In addition to strong dependence on storm type, the simulated precipitation scaling rate itself exhibits a moderate dependence on the magnitude of future warming. For storms characterized by an AR accompanied by an ETC, the future precipitation scaling is near or above the CC rate (0.7–1.4 times CC) for the 2050 simulations and above the CC rate (1.1–1.5 times CC) for the 2100 simulations (Table 3). This increase in precipitation scaling as the magnitude of warming increases from the 2050 to the 2100 climates is consistent with the temperature dependence of precipitation scaling found by Kharin et al. (2013) in the much lower resolution Coupled Model Intercomparison Project Phase 5 (CMIP5) experiments.

Since each of the storm events is characterized by an AR, we investigate how future changes in precipitable water and integrated water vapor transport (IVT) may contribute to the future precipitation changes. Interestingly, the projected future changes in precipitation have little correlation with future changes in precipitable water or IVT. Precipitable water not only increases in the future for all storm events, but increases at a rate exceeding CC (Fig. 11 and Table 3), despite weak or negative future changes in precipitation for storms characterized by an AR only (i.e., storms 2 and 3). The projected decrease in storm-total precipitation for storm 3, despite the increase in precipitable water, suggests that dynamical effects are dominating the thermodynamic changes. The same is true for IVT (Fig. 12 and Table 3), consistent with

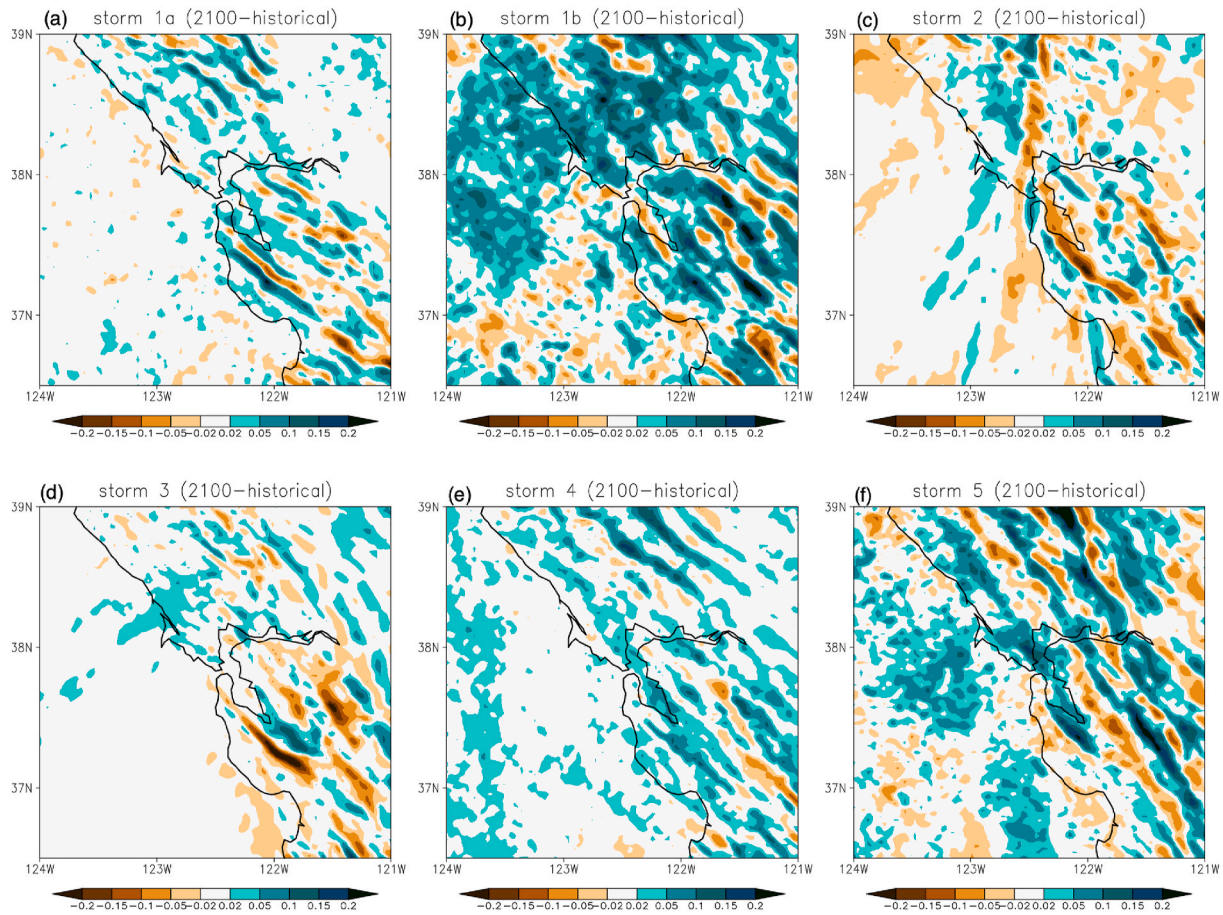

Fig. 13. Future change in positive values only of vertical velocity at 500 hPa (m s^{-1}) from the ensemble mean of the 2100 minus historical simulations on the 3 km resolution domain for (a) storm 1a, (b) storm 1b, (c) storm 2, (d) storm 3, (e) storm 4, (f) storm 5. Vertical velocity for each event is averaged over the same days as in Fig. 9.

Dominguez et al. (2018), indicating that to fully understand future climate change impacts associated with ARs it is necessary to consider not only IVT but also the actual precipitation. Although this may seem surprising, as large values of precipitable water and IVT are often associated with extreme precipitation, they alone are insufficient conditions for precipitation, which also requires a lifting mechanism. This may explain why ARs accompanied by ETCs, which are associated with strong surface convergence, rather than ARs alone, are preferentially projected to experience increased precipitation in the future.

We investigate the hypothesis that the sign of the future precipitation change is linked with dynamical, rather than thermodynamic, changes in the storm events by evaluating the future change in vertical velocity at 500 hPa. We considered the vertical velocity over the Bay Area region shown in Fig. 9a and over land only, to be consistent with the evaluation of precipitation changes. The vertical velocity is also considered over the entire lifetime of the storm event (Table 1). To calculate the vertical velocity change, we set any negative vertical velocity values (i.e., descent) at each point in time and space and for each ensemble member to zero, as the purpose is to evaluate changes in ascent only, which would relate to precipitation. Maps of the future change (2100 minus historical) for the ensemble average of each storm event are shown in Fig. 13, and the Bay Area averaged percent changes are included in Table 3, to help quantify the changes in this relatively noisy variable. For storm events characterized by an AR only, there are areas of substantial decreases in ascent at 500 hPa over the Bay Area (Fig. 13 c and d) in the 2100 simulation relative to the historical, which correspond to future changes of −4.3% and −1.5% for storm 2 and storm 3, respectively, over the Bay Area region (Table 3). On the other hand, there are widespread (Fig. 13a–b and e-f) and substantial (Table 3) increases in ascent at 500 hPa in the 2100 simulations relative to the historical for storm events characterized by a co-occurring AR and ETC. Specifically, for storm events 1, 4, and 5, mid-tropospheric ascent in the 2100 simulation increases by 7.3%–18.3% relative to the historical (Table 3). This supports the idea that the differences in the sign of future precipitation change between AR-only events and co-occurring AR and ETC events are linked with dynamical changes in the storm events (i.e., mid-tropospheric ascent) rather than thermodynamic changes (i.e., precipitable water).

In addition to considering future changes in storm-total precipitation, we evaluated changes in the probability of extreme 3-hourly precipitation rates, which are also important for climate change impacts such as flash flooding. We calculated probability density functions (PDFs) using 3-hourly precipitation data from all model grid points over the Bay Area region and over the lifetime of each storm event, and for each ensemble member (i.e., no spatial, temporal, or ensemble averaging was applied). The calculation is intentionally different from that used for the storm-total precipitation, so that we can retain information regarding extreme rainfall rates, rather than smoothing them out by using area-averaging and ensemble-averaging. We note that the PDFs are plotted for values corresponding to 0.1 inches/3-h (or 2.54 mm/3-h) and greater, in order to be able to clearly see the tails of the extremes, which would otherwise be difficult to see given that near-zero 3-hourly precipitation rates occurred relatively frequently within the region and time considered. The 3-hourly precipitation rates shift toward stronger values in the 2100 simulations for individual ensemble members and the full 10-member ensemble for all storm events, regardless of whether the storm-total precipitation changes were positive or negative (Fig. 14).

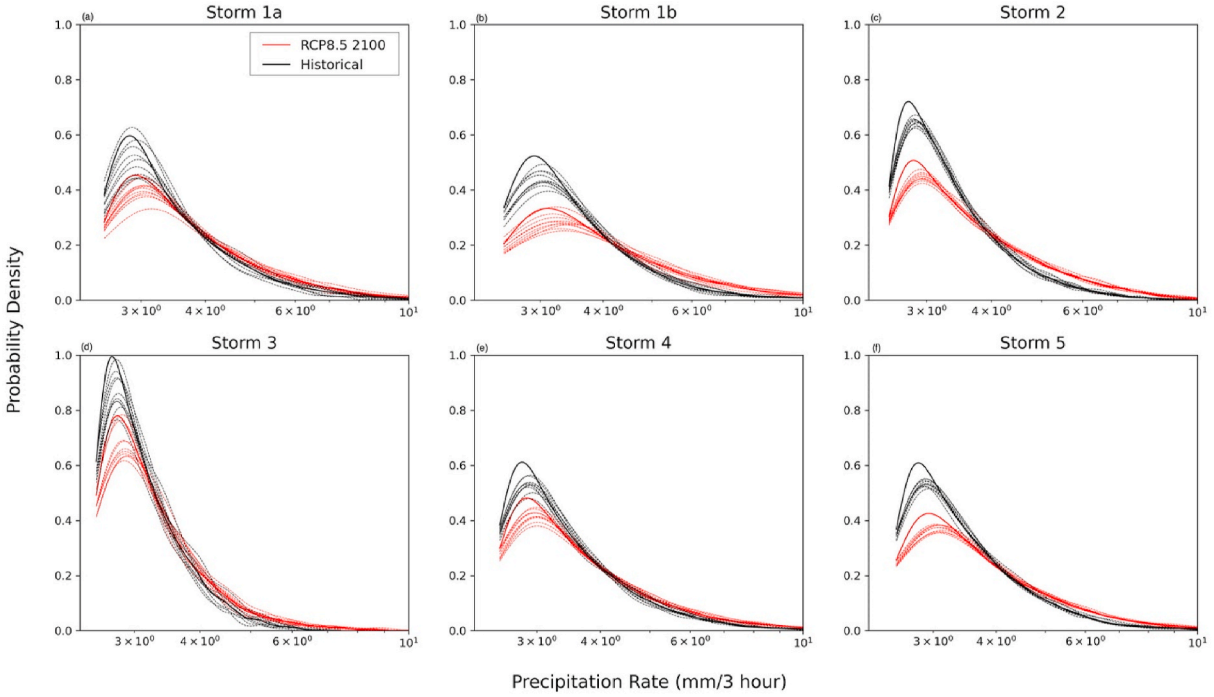

Fig. 14. Probability density functions of 3-hourly precipitation rates (mm/3-h) for precipitation over the San Francisco Bay Area during the storm life time for (a) storm 1a, (b) storm 1b, (c) storm 2, (d) storm 3, (e) storm 4, and (f) storm 5 from the 2100 (red) and historical (black) simulations at 3 km resolution. Dashed lines represent individual ensemble members and solid lines represent the full 10-member ensemble. Note that the x-axis is plotted on the log-scale, and that values are shown for precipitation rates of 2.54 mm/3-h (0.1 inches/3-h) and above only. (For interpretation of the references to color in this figure legend, the reader is referred to the Web version of this article.)

This suggests that the precipitation scaling rate with future temperature warming may be different for storm-total precipitation compared with 3-hourly precipitation. This may be related to differences in the way in which storm-total precipitation and 3-hourly precipitation were considered, with the former quantity area-averaged over the Bay Area domain and ensemble-averaged, and the latter considered using each model gridpoint within the Bay Area domain and each ensemble member. We plan an in-depth analysis of future changes in sub-daily precipitation rates in future work.

4. Discussion and conclusions

Reliable projections of future changes in extreme precipitation are urgently needed to provide decision makers with the best possible information as the climate continues to warm. Future projections are uncertain from state-of-the-art global climate models, as such models require the use of convective parameterization and are typically run at resolutions insufficient to reproduce observed extreme precipitation rates and to properly represent topography, which provides an important lifting mechanism. In this study, with input from stakeholders of the City and County of San Francisco, California, we designed and performed 10-member ensembles of 3 km resolution regional climate model simulations to provide extreme precipitation projections over the San Francisco Bay Area. The simulations consist of hindcasts of five historically impactful extreme precipitation events, which were characterized by either an atmospheric river (AR) alone, or an AR accompanied by an extratropical cyclone (ETC). We then adjusted the greenhouse gas concentrations and prescribed sea-surface temperature and initial and lateral boundary conditions to simulate the historical storm events in future climates, specifically the years 2050 and 2100 under the RCP8.5 emissions scenario. These "storyline" experiments are designed to inform how the magnitude of events like the historical storms could change if similar events occurred in a warmer world. The assumption behind this methodology is that the Bay Area would continue to be impacted by ARs and ARs with ETCs in the future, which is reasonable given the prevalence of such storms. We note that this experimental design does not address future changes in event frequency or shifts in storm tracks, which requires multi-decadal global climate model simulations. Therefore, while this study can provide information on changes in the magnitude of precipitation associated with individual storm events, it is unable to address how precipitation will change overall.

We found that future storm-total precipitation changes depend strongly on storm type, with increases for events associated with an AR accompanied by an ETC (storms 1, 4, and 5) and weak or negative changes for events associated with an AR only (storms 2 and 3). The future precipitation increases in co-occurring AR and ETC events scale at a rate that exceeds the theoretical Clausius Clapeyron scaling of ~6.5% per °C warming, by up to 1.5 times the CC rate. Given that the majority of observed ARs are associated with an ETC, this has important implications for future precipitation impacts over the Bay Area, as it indicates that storm-total precipitation associated with the most common type of storm event may increase by 26–37% in 2100 relative to historical, i.e., up to 9.75% per °C warming. Another interesting finding is that precipitable water and integrated vapor transport increase at similar percentage rates for all storm events, despite the weak or negative precipitation changes for the AR-only events. Although this may seem surprising, as large values of precipitable water and strong IVT are often associated with extreme precipitation, they alone are insufficient conditions for extreme AR precipitation, which also requires a lifting mechanism. Indeed, we found that instead, changes in mid-tropospheric vertical velocity can explain the differences in future storm-total precipitation changes between AR-only compared with co-occurring AR and ETC events. This result highlights that future changes in precipitable water and IVT associated with ARs may not alone be accurate indicators of future changes in precipitation.

For future work it would be useful to consider additional storm events in order to better understand how generalizable the extreme precipitation scaling rates are. In addition, we note that the projections

presented here used one global climate model to provide the future changes in SST and lateral boundary conditions for the 2050 and 2100 experiments. However, this is not as significant a limitation on our findings as it may appear. Changes in extreme precipitation are clearly linked to temperature changes in regions of storm moisture sources. These future temperature changes are highly dependent on emissions scenario, the time frame of interest, and climate sensitivity. If these factors are external to the extreme precipitation scaling rules presented here, decision makers and practitioners can use the scaling rates simulated in this study to estimate local future extreme storm-total precipitation percent changes by simply applying estimated regional warmings at a desired time under a desired emissions scenario for each type of storm event (i.e., AR-only or co-occurring AR and ETC). We note that the scaling rates may be different for daily and sub-daily precipitation extremes, a topic planned for future research. As confidence in future regional temperature projections obtained from downscaled CMIP experiments is significantly higher than for precipitation from such experiments, we maintain that confidence in projected extreme precipitation changes obtained from application of these scaling rules should be considered as higher, subject to the assumption that storm frequency and types does not change.

Author contributions

CMP and MFW conceived the study with input from AR and SL. CMP designed, ran, and analyzed the regional climate model simulations, interpreted results, and wrote the manuscript. EB-H configured the future simulations. MFW assembled global climate model data to perturb future climate simulations. FVM and EB-H contributed to the analysis. MFW, EB-H, and FVW contributed to interpreting results. Storm events were selected by KM, MM, and OY with input from CMP, MFW, and the stakeholder working group. All authors contributed to editing the manuscript.

Declaration of competing interest

The authors declare that they have no known competing financial interests or personal relationships that could have appeared to influence the work reported in this paper.

Acknowledgements

This research was supported by the City and County of San Francisco (CCSF) and used resources of the National Energy Research Scientific Computing Center (NERSC; https://www.nersc.gov; DOI: 10.13039/100017223), a U.S. Department of Energy Office of Science User Facility located at Lawrence Berkeley National Laboratory, operated under Contract No. DE-AC02-05CH11231. This work used the Extreme Science and Engineering Discovery Environment (XSEDE) computing resource Stampede2, which is supported by National Science Foundation grant number ACI-1548562, through allocations ATM190012 and ATM190016. The authors acknowledge the Texas Advanced Computing Center (TACC; http://www.tacc.utexas.edu) at The University of Texas at Austin for providing HPC resources that have contributed to the research results reported within this paper. Support for OY was provided by National Science Foundation Award No. 1541181. FVM performed research under the Berkeley Lab Undergraduate Research (BLUR) program. We are grateful to the stakeholder working group, consisting of members from CCSF agencies, for their input. CESM large ensemble data available at https://www.cesm.ucar.edu/projects/community-projects/LENS/data-sets.html, NARR data available at https://rda.ucar.edu/datasets/ds608.0/, and gridMET data available at http://www.climatologylab.org/gridmet.html. GrADS script color.gs by Chihiro Kodama with color palettes from https://colorbrewer2.org/. County borders on figures enabled by script and shapefiles available at https://www.dropbox.com/s/9gyclikwqhsjaf8/Shapefile.gs and https://www.weather.gov/gis/Counties, respectively. WRF data is available at https://portal.nersc.gov/archive/home/projects/cascade/www/SFPUC. We thank Xuebin Zhang and one anonymous reviewer for their constructive comments which helped improve the manuscript.

References

Abatzoglou, J.T., 2013. Development of gridded surface meteorological data for ecological applications and modelling. Int. J. Climatol. 33, 121–131.
Algarra, I., Nieto, R., Ramos, A.M., Eiras-Barca, J., Trigo, R.M., Gimeno, L., 2020. Significant increase of global anomalous moisture uptake feeding landfalling Atmospheric Rivers. Nat. Commun. 11, 5082.
Allen, M.R., Ingram, W.J., 2002. Constraints on future changes in climate and the hydrologic cycle. Nature 419, 224–232.
Ali, H., Fowler, H.J., Lenderink, G., Lewis, E., Pritchard, D., 2021. Consistent large-scale response of hourly 26 extreme precipitation to temperature variation over land. Geophys. Res. Lett. https://doi.org/10.1029/2020GL090317.
Baggett F., C., Barnes A., E., Maloney D., E., Mundhenk D., B., 2017. Advancing atmospheric river forecasts into subseasonal-to-seasonal time scales. Geophysical Research Letters 44, 7528–7536. https://doi.org/10.1002/2017GL074434.
Ban, N., Schmidli, J., Schär, C., 2015. Heavy precipitation in a changing climate: does short-term summer precipitation increase faster? Geophys. Res. Lett. 42, 1165–1172.
Bercos-Hickey, E., Patricola, C.M., Gallus Jr., W.A., 2021. Anthropogenic Influences on Tornadic Storms. Journal of Climate 34 (22), 8989–9006.
Berg, P., Moseley, C., Haerter, J.O., 2013. Strong increase in convective precipitation in response to higher temperatures. Nat. Geosci. 6, 181–185.
Bullister, J.L.. Atmospheric histories (1765-2015) for CFC-11, CFC-12, CFC-113, CCl4, SF6 and N2O. NDP-095. http://cdiac.ess-dive.lbl.gov/ftp/oceans/CFC_ATM_Hist/CFC_ATM_Hist_2015/(Carbon Dioxide Information Analysis Center, Oak Ridge National Laboratory, US Department of Energy, 2015).
Chen, F., Dudhia, J., 2001. Coupling an advanced land-surface/hydrology model with the Penn State/NCAR MM5 modeling system. Part I: model description and implementation. Mon. Weather Rev. 129, 569–585.
DeFlorio, M.J., Waliser E., D., Ralph M., F., Guan, B., et al., 2019. Experimental subseasonal-to-seasonal (S2S) forecasting of atmospheric rivers over the western United States. J. Geophys. Res. 124, 11242–11265.
Dettinger, M., 2011. Climate change, atmospheric rivers, and floods in California - a multimodel analysis of storm frequency and magnitude Changes1. J. Am. Water Resour. Assoc. 47, 514–523.
Di Luca, A., Argüeso, D., Sherwood, S., Evans, J.P., 2021. Evaluating precipitation errors using the environmentally conditioned intensity-frequency decomposition method. J. Adv. Model. Earth Syst. 13, 1–22. https://doi.org/10.1029/2020MS002447.
Dominguez, F., Dall'erba, S., Huang, S., Avelino, A., et al., 2018. Tracking an atmospheric river in a warmer climate: from water vapor to economic impacts. Earth Syst. Dyn. 9, 249–266.
Espinoza, V., Waliser, D.E., Guan, B., Lavers, D.A., Martin Ralph, F., 2018. Global analysis of climate change projection effects on atmospheric rivers. Geophys. Res. Lett. 45, 4299–4308. https://doi.org/10.1029/2017gl076968.
Fowler, H.J., Lenderink, G., Prein, A.F., Westra, S., Allan, R.P., Ban, N., et al., 2021. Anthropogenic intensification 23 of short-duration rainfall extremes. Nat. Rev. Earth Environ. 2, 107–122. https://doi.org/10.1038/s43017-020-00128-6.
Gao, Y., Lu, J., Leung, L.R., Yang, Q., Hagos, S., Qian, Y., 2015. Dynamical and thermodynamical modulations on future changes of landfalling atmospheric rivers over western North America. Geophys. Res. Lett. 42, 7179–7186.
Gao, Y., Lu, J., Leung, L.R., 2016. Uncertainties in projecting future changes in atmospheric rivers and their impacts on heavy precipitation over europe. J. Clim. 29, 6711–6726.
Gershunov, A., Shulgina, T., Clemesha E.S., R., Guirguis, K., et al., 2019. Precipitation regime change in western North America: the role of atmospheric rivers. Sci. Rep. 9, 9944.
Gershunov, A., Shulgina, T., Ralph, F.M., Lavers, D.A., Rutz, J.J., 2017. Assessing the climate-scale variability of atmospheric rivers affecting western North America. Geophys. Res. Lett. 44, 7900–7908. https://doi.org/10.1002/2017gl074175.
Gimeno, L., Nieto, R., Vázquez, M., Lavers, D., 2014. Atmospheric rivers: a mini-review. Front. Earth Sci. China 2, 2.
Gutmann, et al., 2018. Changes in hurricanes from a 13 Year convection permitting pseudo-global warming simulation. J. Clim. 31, 3643–3657. https://doi.org/10.1175/JCLI-D-17-0391.1.
Haerter, J.O., Berg, P., Hagemann, S., 2010. Heavy rain intensity distributions on varying time scales and at different temperatures. J. Geophys. Res. 115 https://doi.org/10.1029/2009jd013384.
Hagos, S.M., Ruby Leung, L., Yoon, J., Lu, J., Gao, Y., 2016. A projection of changes in landfalling atmospheric river frequency and extreme precipitation over western North America from the Large Ensemble CESM simulations. Geophys. Res. Lett. 43, 1357–1363. https://doi.org/10.1002/2015gl067392.
Hagos, S., Ruby Leung, L., Garuba, O., Patricola, C.M., 2021. Influence of background divergent moisture flux on the frequency of north pacific atmospheric rivers. J. Clim. 1, 1–33.
Hardwick Jones, R., Westra, S., Sharma, A., 2010. Observed relationships between extreme sub-daily precipitation, surface temperature, and relative humidity. Geophys. Res. Lett. 37 https://doi.org/10.1029/2010gl045081.
Hatsuzuka, D., Sato, T., Higuchi, Y., 2021. Sharp rises in large-scale, long-duration precipitation extremes with higher temperatures over Japan. npj Climate and Atmospheric Science 4, 1–7.

Held, I.M., Soden, B.J., 2006. Robust responses of the hydrological cycle to global warming. J. Clim. 19, 5686–5699.
Huang, H., Patricola, C.M., Bercos-Hickey, E., Zhou, Y., Rhoades, A., Risser, M.D., Collins, W.D., 2021. Sources of subseasonal-to-seasonal predictability of atmospheric rivers and precipitation in the western United States. J. Geophys. Res. 126 https://doi.org/10.1029/2020jd034053.
Huang, X., Swain, D.L., Hall, A.D., 2020. Future precipitation increase from very high resolution ensemble downscaling of extreme atmospheric river storms in California. Sci. Adv. 6, eaba1323.
Ikeda, K., Rasmussen, R., Liu, C., et al., 2021. Snowfall and snowpack in the Western U.S. as captured by convection permitting climate simulations: current climate and pseudo global warming future climate. Clim. Dynam. 57, 2191–2215. https://doi.org/10.1007/s00382-021-05805-w.
Ito, R., Takemi, T., Arakawa, O., 2016. A possible reduction in the severity of typhoon wind in the northern part of Japan under global warming: a case study. Solaiat 12, 100–105.
Kain, J.S., 2004. The Kain-Fritsch convective parameterization: an update. J. Appl. Meteorol. 43, 170–181.
Kain, J.S., Fritsch, J.M., 1990. A one-dimensional entraining/detraining plume model and its application in convective parameterization. J. Atmos. Sci. 47, 2784–2802.
Kay, J.E., Deser, C., Phillips, A., Mai, A., et al., 2015. The community Earth system model (CESM) large ensemble project: a community resource for studying climate change in the presence of internal climate variability. Bull. Am. Meteorol. Soc. 96, 1333–1349. https://doi.org/10.1175/bams-d-13-00255.1.
Kelley, G., Sweiss, F., Coauthors, 2016. San Francisco Sea level rise action plan. https://sfpublicworks.org/sites/default/files/2%20160309_SLRAP_Executive%20Summary_ED_0.pdf 16.
Kharin, V.V., Zwiers, F.W., Zhang, X., Wehner, M., 2013. Changes in temperature and precipitation extremes in the CMIP5 ensemble. Clim. Change 119, 345–357.
Lackmann, G.M., 2015. Hurricane sandy before 1900 and after 2100. Bull. Am. Meteorol. Soc. 96, 547–560.
Lamjiri A., M., Dettinger D., M., Ralph M., F., Oakley S., N., Rutz J., J., 2018. Hourly analyses of the large storms and atmospheric rivers that provide most of California's precipitation in only 10 to 100 hours per year. San Francisco Estuary and Watershed Science 16 (4). https://doi.org/10.15447/sfews.2018v16iss4art1.
Lenderink, G., van Meijgaard, E., 2008. Increase in hourly precipitation extremes beyond expectations from temperature changes. Nat. Geosci. 1, 511–514.
Lenderink, G., Mok, H.Y., Lee, T.C., van Oldenborgh, G.J., 2011. Scaling and trends of hourly precipitation extremes in two different climate zones – Hong Kong and The Netherlands. Hydrol. Earth Syst. Sci. 15, 3033–3041.
Lenderink, G., Barbero, R., Loriaux, J.M., Fowler, H.J., 2017. Super-clausius–clapeyron scaling of extreme hourly convective precipitation and its relation to large-scale Atmospheric conditions. J. Clim. 30, 6037–6052. https://doi.org/10.1175/jcli-d-16-0808.1.
Meinshausen, M., Smith, S.J., Calvin, K., et al., 2011. The RCP greenhouse gas concentrations and their extensions from 1765 to 2300. Climatic Change 109, 213.
Mesinger, F., Dimego, G., Kalnay, E., Mitchell, K., et al., 2006. North American regional reanalysis. Bull. Am. Meteorol. Soc. 87, 343–360.
Mlawer, E.J., Taubman, S.J., Brown, P.D., Iacono, M.J., Clough, S.A., 1997. Radiative transfer for inhomogeneous atmosphere: RRTM, a validated correlated-k model for the longwave. J. Geophys. Res. 102 (D14), 16663–16682.
Molnar, P., Fatichi, S., Gaál, L., Szolgay, J., Burlando, P., 2015. Storm type effects on super Clausius–Clapeyron scaling of intense rainstorm properties with air temperature. Hydrol. Earth Syst. Sci. 19, 1753–1766.
Mundhenk D., B., Barnes A., E., Maloney D., E., Baggett F., C., 2018. Skillful empirical subseasonal prediction of landfalling atmospheric river activity using the Madden–Julian oscillation and quasi-biennial oscillation. npj Climate and Atmospheric Science 1 (1). https://doi.org/10.1038/s41612-017-0008-2.
Nakamura, R., Shibayama, T., Esteban, M., Iwamoto, T., 2016. Future typhoon and storm surges under different global warming scenarios: case study of typhoon Haiyan (2013). Nat. Hazards 82, 1645–1681.
Pall, P., Allen, M.R., Stone, D.A., 2007. Testing the Clausius–Clapeyron constraint on changes in extreme precipitation under CO2 warming. Clim. Dynam. 28, 351–363.
Pall, P., Patricola, C.M., Wehner, M.F., Stone, D.A., Paciorek, C.J., Collins, W.D., 2017. Diagnosing conditional anthropogenic contributions to heavy Colorado rainfall in September 2013. Weather Clim. Extrem. 17, 1–6. https://doi.org/10.1016/j.wace.2017.03.004.
Patricola, C.M., Cook, K.H., 2010. Northern African climate at the end of the twenty-first century: an integrated application of regional and global climate models. Clim. Dynam. 35, 193–212. https://doi.org/10.1007/s00382-009-0623-7.
Patricola, C.M., Cook, K.H., 2013. Mid-twenty-first century warm season climate change in the Central United States. Part I: regional and global model predictions. Clim. Dynam. 40, 551–568. https://doi.org/10.1007/s00382-012-1605-8.
Patricola, C.M., Wehner, M.F., 2018. Anthropogenic influences on major tropical cyclone events. Nature 563, 339–346. https://doi.org/10.1038/s41586-018-0673-2.
Patricola, C.M., O'Brien, J.P., Risser, M.D., Rhoades, A.M., O'Brien, T.A., Ullrich, P.A., Stone, D.A., Collins, W.D., 2020. Maximizing ENSO as a source of western US hydroclimate predictability. Clim. Dynam. 54, 351–372.
Payne, A.E., Demory E., M., Leung R., L., Ramos M., A., et al., 2020. Responses and impacts of atmospheric rivers to climate change. Nat. Rev. Earth Environ. 1, 143–157.
Payne, A.E., Magnusdottir, G., 2015. An evaluation of atmospheric rivers over the North Pacific in CMIP5 and their response to warming under RCP 8.5. J. Geophys. Res. 120, 11,173–11,190.
Pierce, D.W., Cayan R., D., Das, T., Maurer P., E., et al., 2013. The key role of heavy precipitation events in climate model disagreements of future annual precipitation changes in California. J. Clim. 26, 5879–5896.
Polade, S.D., Gershunov, A., Cayan, D.R., Dettinger, M.D., Pierce, D.W., 2017. Precipitation in a warming world: assessing projected hydro-climate changes in California and other Mediterranean climate regions. Sci. Rep. 7, 10783.
Prein, A.F., Rasmussen, R.M., Ikeda, K., Liu, C.H., Clark, M.P., Holland, G.J., 2017. The future intensification of hourly precipitation extremes. Nat. Clim. Change 7, 48–52. https://doi.org/10.1038/nclimate3168.
Ralph, F.M., Rutz J., J., Cordeira M., J., Dettinger, M., et al., 2019. A scale to characterize the strength and impacts of atmospheric rivers. Bull. Am. Meteorol. Soc. 100, 269–289. https://doi.org/10.1175/bams-d-18-0023.1.
Rasmussen, R., Liu, C., Ikeda, K., Gochis, D.J., Yates, D., Chen, F., Tewari, M., Barlage, M., Dudhia, J., Yu, W., Miller, K., Arsenault, K., Grubišić, V., Thompson, G., Gutmann, E., 2011. High-resolution coupled climate runof simulations of seasonal snowfall over Colorado: a process study of current and warmer climate. J. Clim. 24, 3015–3048.
Rhoades, A.M., Jones D., A., Srivastava, A., Huang, H., et al., 2020. The shifting scales of western U.s. landfalling atmospheric rivers under climate change. Geophys. Res. Lett. 47 https://doi.org/10.1029/2020gl089096.
Schär, C., Frei, C., Lüthi, D., Davies, H.C., 1996. Surrogate climate-change scenarios for regional climate models. Geophys. Res. Lett. 23, 669–672. https://doi.org/10.1029/96gl00265.
Shields, C.A., Kiehl, J.T., 2016. Atmospheric river landfall-latitude changes in future climate simulations. Geophys. Res. Lett. 43, 8775–8782. https://doi.org/10.1002/2016gl070470.
Shields, C.A., Rutz J., J., Leung, L.-Y, Ralph M., F., et al., 2018. Atmospheric river tracking method Intercomparison project (ARTMIP): project goals and experimental design. Geosci. Model Dev. (GMD) 11, 2455–2474.
Skamarock, W.C., Klemp, J.B., 2008. A time-split nonhydrostatic atmospheric model for weather research and forecasting applications. J. Comput. Phys. 227, 3465–3485.
Sun, Q., Zhang, X., Zwiers, F., Westra, S., Alexander, L.V., 2021. A global, continental, and regional analysis of changes in extreme precipitation. J. Clim. 34 (1), 243–258. https://doi.org/10.1175/JCLI-D-19-0892.1.
Swain, D.L., Langenbrunner, B., David Neelin, J., Hall, A., 2018. Increasing precipitation volatility in twenty-first-century California. Nat. Clim. Change 8, 427–433. https://doi.org/10.1038/s41558-018-0140-y.
Takayabu, I., Hibino, K., Sasaki, H., Shiogama, H., Mori, N., Shibutani, Y., Takemi, T., 2015. Climate change effects on the worst-case storm surge: a case study of Typhoon Haiyan. Environ. Res. Lett. 10, 064011.
Tsutsumi, Y., Mori, K., Hirahara, T., Ikegami, M., Conway, T.J., 2009. Technical Report of Global Analysis Method for Major Greenhouse Gases by the World Data Center for Greenhouse Gases. World Meteorological Organization. GAW Report No. 184. https://www.wmo.int/pages/prog/arep/gaw/documents/TD_1473_GAW184_web.pdf.
Utsumi, N., Seto, S., Kanae, S., Maeda, E.E., Oki, T., 2011. Does higher surface temperature intensify extreme precipitation? Geophys. Res. Lett. 38 https://doi.org/10.1029/2011gl048426.
Warner, M.D., Mass, C.F., Salathé, E.P., 2015. Changes in winter atmospheric rivers along the North American west coast in CMIP5 climate models. J. Hydrometeorol. 16, 118–128.
Wehner, M., Gleckler, P., Lee, J., 2020. Characterization of long period return values of extreme daily temperature and precipitation in the CMIP6 models: Part 1, model evaluation. Weather Clim. Extrem. 30, 100283.
Wehner, M.F., Reed A., K., Li, F., et al., 2014. The effect of horizontal resolution on simulation quality in the Community Atmospheric Model, CAM5.1. J. Adv. Model. Earth Syst. 6, 980–997.
Wehner, M.F., Zarzycki, C., Patricola, C.M., 2019. In: Collins, J.M., Walsh, K. (Eds.), Estimating the Human Influence on Tropical Cyclone Intensity as the Climate Changes. *Hurricane Risk*. Springer International Publishing, pp. 235–260.
Westra, S., Fowler J., H., Evans P., J., Alexander V., L., Berg, P., Johnson, F., Kendon J., E., Lenderink, G., Roberts M., N., 2014. Future changes to the intensity and frequency of short-duration extreme rainfall. Rev. Geophys. 52, 522–555. https://doi.org/10.1002/2014RG000464.
Wood, R.R., Ludwig, R., 2020. Analyzing internal variability and forced response of subdaily and daily extreme precipitation over Europe. Geophys. Res. Lett. 47 https://doi.org/10.1029/2020gl089300.
Zhang, Z., Ralph, F.M., Zheng, M., 2019. The relationship between extratropical cyclone strength and atmospheric river intensity and position. Geophys. Res. Lett. 46, 1814–1823.
Zhao, M., 2020. Simulations of atmospheric rivers, their variability, and response to global warming using GFDL's new high-resolution general circulation model. J. Clim. 33, 10287–10303.
Zhou, Y., Kim M., H., 2018. Prediction of atmospheric rivers over the North Pacific and its connection to ENSO in the North American multi-model ensemble (NMME). Climate Dynamics 51, 1623–1637. https://doi.org/10.1007/s00382-017-3973-6.